TRENDS IN SCIENCES 2025; 22(10): 10420
https://doi.org/10.48048/tis.2025.10420 RESEARCH ARTICLE

β-Sitosterol from *Piper crocatum*: A Dual-Action Antifungal and Antibacterial Agent for Oral Infections

Norma Aura Tristyaningrum, Tati Herlina and Dikdik Kurnia*

Department of Chemistry, Faculty of Mathematics and Natural Science, Universitas Padjadjaran, Sumedang 45363, Indonesia.

(*Corresponding author's e-mail: dikdik.kurnia@unpad.ac.id)

Received: 21 April 2025, Revised: 26 May 2025, Accepted: 6 June 2025, Published: 20 July 2025

Abstract

The high prevalence of antibiotic resistance and oral health problems has sparked research into the development of new antimicrobial medications. The habit of chewing *Piper crocatum* leaves among Asians has driven this research, leading to the isolation of a bioactive compound. From the methanol extract, the compound *β*-sitosterol, a phytosterol, was isolated for the 1st time from this leaf, this compound has broad medicinal properties, including antifungal and antibacterial effects. The structure of the *β*-sitosterol compound was validated by ^{1}H-NMR, ^{13}C-NMR, IR and MS spectroscopy. Using the broth dilution method, we determined the minimum inhibitory concentration (MIC) and minimum bactericidal concentration (MBC) of *β*-sitosterol against the oral pathogens *Streptococcus mutans*, *Streptococcus sanguinis*, and *Candida albicans*. The MIC values were 312.5 ± 0.16 µg/mL for *S. mutans*, 625 ± 0.11 µg/mL for *S. sanguinis*, and 625 ± 0.15 µg/mL for *C. albicans*, respectively. To support these data, we also predicted the potential of the compounds as specific enzyme inhibitors and their absorption, distribution, metabolism, excretion and toxicity (ADMET) properties of the compound and their derivatives by *in silico*. This study revealed that the derivative *β*-sitosterol-3-O-*β*-d-glucoside is the most potent as inhibitor of GbpC and SrtC, as antibacterial properties, and is an antifungal agent against Sap5 and CYP51. By preventing the formation of harmful oral bacteria and fungi, the *β*-sitosterol found in *P. crocatum* leaves and their derivatives can therefore potentially function as an antibacterial agent.

Keywords: *β*-sitosterol, Phytosterol, *Piper crocatum*, Bioactivity-guided, Antibacterial, Antifungal

Introduction

Oral health plays a crucial role in maintaining general health [1]. Preventing dental problems including cavities and periodontal diseases, as well as their wider effects on systemic health, requires maintaining good oral health [2,3]. Research has demonstrated that poor oral hygiene increases the risk of serious conditions, including cardiovascular disease, diabetes, and respiratory infections [4-6]. Among these, certain bacteria and fungi play significant roles in either maintaining or compromising oral health. *Streptococcus mutans* is often associated with its capacity to create acids from the fermentation of carbohydrates, which results in tooth damage and dental caries [7]. By altering the composition of biofilms and interacting with other oral pathogens, *S. sanguinis* can affect the oral environment [8]. Furthermore, a fungus called *Candida albicans* can cause oral infections such as thrush, particularly in people on antibiotics or those with weakened immune systems [9-11].

The management of oral diseases often involves the use of antibiotics and antifungal agents to combat bacterial and fungal infections [12,13]. However, the increasing prevalence of antibiotic and antifungal resistance poses a significant challenge in this context [14]. Commonly used antibiotics, such as penicillins and cephalosporins, are resistant to bacteria such as *Streptococcus* and *Staphylococcus*, while macrolides and fluoroquinolones are also resistant in certain strains

[15,16]. Similarly, antifungal agents like azoles are becoming less effective against fungi such as *C. albicans*, which can develop resistance through mechanisms involving biofilms and genetic mutations [17,18]. As a result, strategies to combat resistance, including the development of new antimicrobial agents, are urgently needed [19-22]. This study aims to explore this challenge by searching for compounds abundant in nature that can be potential antimicrobials with multitarget bioactivity against *S. mutans*, *S. sanguinis*, and *C. albicans*.

Among natural compounds, β-sitosterol, a phytosterol commonly found in plant-based foods, has garnered attention for its potential health benefits, including lowering cholesterol levels and managing benign prostatic hyperplasia [23,24]. Recent studies have also investigated its antimicrobial properties, revealing moderate antibacterial activity against certain pathogens [24,25]. While its effectiveness as a standalone antimicrobial agent is limited compared with that of conventional antibiotics, β-sitosterol shows promise when used in synergistic combinations with existing drugs [26]. The antimicrobial potential of β-sitosterol against *C. albicans*, *S. mutans*, and *S. sanguinis* remains underexplored in current research.

The formation of biofilms by both bacteria and fungi further complicates treatment by protecting these microorganisms from the effects of antibiotics and antifungals [27]. An essential stage in the development of dental caries is the creation and maintenance of biofilms on the tooth surface, which are facilitated by the GbpC enzyme from *S. mutans* [28]. Sap5 facilitates adhesion and proteolysis during *C. albicans* biofilm formation, whereas SrtC contributes to protein anchoring and matrix synthesis in *S. sanguinis* [29,30].

Materials and methods

General experimental procedures

NMR spectra were captured using a Bruker 700 MHz device. Additionally, HR-ESI-MS spectra were acquired by attaching a quadrupole time of flight mass spectrometer (Xevo G2-XS QTOF, Waters Corp.) to a Waters ACQUITY UPLC system (Waters Corp., Milford, MA). RP-18 gel (63 - 212 µm, Fujifilm Wako, Osaka, Japan) and silica gel (0.063 - 0.2 mm, Merck, Darmstadt, Germany) were used for column chromatography (CC). The RP-18 F254S (0.25 mm, Merck) and 60 F254 (0.25 mm, Merck) precoated silica gel plates were utilized for thin layer chromatography (TLC). Sample spots were visualized by heating and spraying with 10% aqueous H_2SO_4.

Plant materials

Fresh leaves of *Piper crocatum* (Ruiz and Pav.) were gathered in September 2022 from Cikarang Barat, Bekasi, Jawa Barat, Indonesia. The plant material was identified in the Biosystematics and Molecular Laboratory at the Department of Biology, Faculty of Mathematics and Natural Sciences, Universitas Padjadjaran, Sumedang, Indonesia with number 93/LBM/IT/9/2022.

Extraction and isolation

The dried and cut leaves of *P. crocatum* (15 kg) were extracted with 150 L of methanol through maceration at room temperature (25 °C) for 3 days. The collected methanol filtrate was evaporated under reduced pressure (Buchi Rotavapor R-100, Switzerland), to yield a solid extract (25 g). The concentrated *P. crocatum* methanol extract was then separated by column chromatography using Silica G 60 stationary phase (0.063 - 0.200 mm) with solvent *n*-hexane and ethyl acetate with an increasing 10% gradient, from 100% *n*-hexane to 100% ethyl acetate to afford in a total of 11 fractions (**Fr.A-K**). With the bioactivity-guided method, each fraction was then tested against *S. mutans*, *S. sanguinis*, and *C. albicans* microorganisms by disc diffusion [31,32]. The results obtained are listed in **Table S1** in the Supplementary information, showing that **Fr.C** has the most active activity against all microbes. **Fr.C** was then purified by column chromatography, eluted with a solvent gradient system of 100% n-hexane to a mixture of n-hexane (95%) in ethyl acetate with a gradient of 0.5%. until 21 subfractions (**Fr.C-1** to **Fr.C-21**) were obtained. Subfractions **Fr.C.13** (29.9 mg) and Fr.C.14 (**55.5 mg**) were combined, and purified with methanol-water solvent, and β-sitosterol (**1**) was eluted as a pure compound in 10% methanol in water.

Microbial strains and culture media

The American Type Culture Collection (ATCC) standard strains *Streptococcus mutans* ATCC 25175, *S. sanguinis* ATCC 10556, and *Candida albicans* ATCC

10231 were employed. Mueller-Hinton agar (MHA) and brain heart infusion (BHI) were used as the culture and assay media for bacteria. Potato dextose broth (Sigma-Aldrich, US) and potato dextrose agar (PDA) were used as the media for the fungi *C. albicans*. Before testing, stock cultures of bacterial strains were grown in the proper medium at 37 °C for 24 h. The turbidity of the bacterial suspension was then adjusted to 0.5 McFarland standard using a Biochrom microplate reader set to 620 nm in wavelength. This resulted in a final concentration of 10^7 CFU/mL [33].

Antimicrobial assay

The fractions (**Fr.A-K**) with antibacterial activity were screened via the disk diffusion method. Fractions were prepared with a concentration of 2%, and the positive control, chlorhexidine (Sigma-Aldrich, US), was utilized. A 5 mL brain heart infusion (BHI) medium (Sigma-Aldrich, US) was inoculated with 100 µL of bacteria. Following a 48 h incubation period at 37 °C, bacterial strains were tested at 620 nm to meet the 0.5 McFarland standard. An aliquot of 100 µL bacterial suspension was spread evenly onto agar medium (Sigma-Aldrich, USA) to assess the zone of inhibition. Each of the fractions and chlorhexidine was dripped for 20 µL on a paper disk (6 mm, Grainger approved, Origin, USA). The paper disks were subsequently cultured for 24 h at 37 °C on a nutritional agar medium [34].

The MIC of compound 1 was assessed via the broth microdilution method. To perform the MIC assay, 100 µL of broth medium was added to each well of a 96-well microplate (NEST Biotechnology, Wuxi, China). A solvent volume of 100 µL was added to columns A-1, B-1, E-1, and F-1, while 100 µL of compound **1** with an initial concentration of 2500 µg/mL was added to columns C-1, D-1, G-1, and H-1. Serial dilutions were performed from columns 1 to 12 via a microdilution technique. In addition, 5 µL of bacterial suspension was added to columns E to H. After incubation for 48 h at 37 °C, the optical density was measured using a microplate reader (Biochrom Ltd., Cambridge, UK) at 620 nm. Then, to determine the minimum bactericidal concentration (MBC) or minimum fungicidal concentration (MFC), each solution including the media, the compound, and bacteria in the microplate (columns G and H) was subsequently distributed over an agar medium and incubated for 48 h at 37 °C [32].

Ramachandran plot for enzyme validation

Ramachandran's plots were used to assess the structural accuracy of the enzymes in this study. Each 3-dimensional structure Gbp C (PDB ID: 6CAM), Srt C (PDB ID: 8GR6), Sap 5 (PDB ID: 2QZX), and CYP51 (PDB ID: 5TZ1) were input in .pdb format on the PROCHECK SAVES v6.1 by the UCLA web server (https://saves.mbi.ucla.edu/) [35].

Molecular docking study

The crystal structures of the target enzymes, including their crystal ligands were retrieved from the RCSB Protein Data Bank (PDB) (https://www.rcsb.org/) in .pdb format. The PDB IDs for each enzyme are as follows: Glucan binding protein C from *Streptococcus mutans* (PDB ID: 6CAM), sortase C from *Streptococcus sanguinis* (PDB ID: 8GR6), Sap 5 from *Candida albicans* (PDB ID: 2QZX), and sterol 14-alpha demethylase enzyme from *C. albicans* (PDB ID: 5TZ1). The receptors are separated from water, ions, and other impurities and saved in .pdb format. β-sitosterol, a compound isolated in *P. crocatum*, that was tested as a ligand *(*CID 222284*)* and its derivatives, 7β-hydroxysitosterol (CID 12309569), β-sitosterol-3-O-β-d-glucoside (CID 12309057), and stigmastanol (CID 241572) was obtained from Pubchem (https://pubchem.ncbi.nlm.nih.gov/) and the energy is minimized with Chemdraw 3D. Kollman partial charges for protein molecules were applied by Autodock 4.0 to create the search grid box and.pdbqt files before the structures were saved as.pdbqt files [36].

The coordinates of the receptor target were determined using a grid box search method, with a focus on the crystal ligands. Redocking was conducted after separating the ligands from the macromolecules to optimize the molecular docking method. The optimization results demonstrated that the docking parameters yielded a Root Mean Square Deviation (RMSD) value of ≤ 2.0 Å, confirming the validity of the grid box [37,38]. The GbpC grid box was X: 236.063, Y: –26.596, Z: 12.498 with box size 40×40×40 Å. The Srt C grid box was X: –2.378, Y: –10.837, Z: –12.165 with box size 40×40×40 Å. The Sap5 grid box was X: –2.378, Y: –10.837, Z: –12.165 with box size 40×50×40

Å. The CYP51 was X: 70.486, Y: 65.237, Z: 4.453 with box size 40×40×40 Å. Subsequently, docking was performed using a genetic algorithm with 100 runs with Autodock 4.0. After docking, the protein and ligand complexes with the best energy were visualized with BIOVIA Discovery Studio [39].

ADMET prediction and drug-likeness analysis

ADME (absorption, distribution, metabolism, and excretion) predictions were analyzed on the pkCSM web server (biosig.lab.uq.edu.au/pkcsm/), while drug-likeness predictions were completed from the SwissADME web server (http://www.swissadme.ch/) [40,41]. Further ADMET profiling was conducted using ADMETlab 3.0 (https://admetmesh.scbdd.com/), to predict toxicity-related parameters, including plasma protein binding (PPB), volume of distribution (VD), clearance (CL), hERG inhibition, AMES toxicity, hepatotoxicity [42,43].

Molecular dynamics simulation

Among the enzyme-ligand complexes evaluated through molecular docking, the complex with lowest binding free energy and the most stable docking pose compared to the other candidates was selected for molecular dynamics (MD) simulations. The partial atomic charges of *β*-sitosterol-3-O-glucoside was calculated using the semi-empirical quantum mechanical Austin Model 1-Bond Charge Correction (AM1-BCC) method, implemented in the antechamber module of AmberTools21. The topology for the ligand was generated using the Generalized Amber Force Fields 2 (GAFF2), and the complex was solvated in a box of 10 Å with TIP3P water molecules. Counter ions (Na^+ and Cl^-) were added to attain a salt concentration of 0.15 M using the tleap utility in AmberTools21.

Molecular dynamics simulations for each protein-ligand complex were conducted using GPU-accelerated Particle-Mesh Ewald Molecular Dynamics (PMEMD) with periodic boundary conditions in Amber20 software27. The procedure began with 2 sequential energy minimization steps: Initially, a positional restraint of 25 kcal mol^{-1} $Å^{-2}$ was applied to the protein-ligand complex, followed by a reduction of the restraint to 5 kcal mol^{-1} $Å^{-2}$ in the 2nd step. The system temperature was then increased to 300 K under an NVT (Number-Volume-Temperature) ensemble for 50 ps. Subsequently, the simulation switched to an NPT (Number-Pressure-Temperature) ensemble to equilibrate the system density to 1 g cm^{-3} over 50 ps. During the following NVT equilibration, restraints on the solute were decreased incrementally by 1 kcal mol^{-1} $Å^{-2}$ every 50 ps until completely removed. Production molecular dynamics simulations were performed for 100 ns at 300 K under NPT conditions to generate trajectories for each system. Root Mean Square Deviation (RMSD) and Root Mean Square Fluctuation (RMSF) analyses were performed using R programming language to evaluate the complex's stability and inhibitory potential throughout the simulation.

Results and discussion

Chemical characterization of *β*-sitosterol (1)

The isolated compound *β*-sitosterol (**1**), was white crystal (65 mg) with ES- *m/z* 413.27; IR (in KBr) ν_{max} 3439, 3072, 2937, 2851, 1639, 1464, 1378, 1054, and 924 cm^{-1}. The ^1H and ^{13}C-NMR shifts of compound **1** are summarized in **Table 1**. The ^{13}C-NMR (**Figure S3** in Supplementary Information) and DEPT displayed 29 carbon signals for 6 methyl carbons (δ_C 11.9 C-18, 19.1 C-19, 18.9 C-21, 21.3 C-26, 19.5 C-27, and 12.0 C-29), 11 methylene carbons (δ_C 37.3 C-1, 31.7 C-2, 42.2 C-4, 31.9 C-7, 21.2 C-11, 39.8 C-12, 24.4 C-15, 28.3 C-16, 33.9 C-22, 26.1 C-23, and 23.1 C-28), 8 methine carbons (δ_C 71.9 C-3, 31.9 C-8, 50.2 C-9, 56.0 C-14, 56.1 C-17, 36.2 C-20, 45.9 C-24, and 29.2 C-25), 3 quaternary carbons (δ_C 140.8 C-5, 36.6 C-10, and 42.4 C-13), and 1 olefinic methine carbon (δ_C 121.8 C-6). ^1H-NMR (**Figure S4**) revealed 6 methyl protons (δ_H 0.84 H-18, 0.82 C-19, 0.92 H-21, 0.83 H-26, 0.83 H-27, and 0.83 H-29), 11 methylene protons (δ_H 1.85 H-1, 1.95 H-2, 2.30 H-4, 1.99 H-7, 1.02 H-11, 1.16 H-12, 1.58 H-15, 1.09 H-16, 1.34 H-22, 1.16 H-23, and 1.25 H-28), and 9 methine protons (δ_H 3.52 H-3, 5.36 H-6, 2.02 H-8, 0.95 H-9, 1.01 H-14, 1.14 H-17, 1.35 H-20, 0.94 C-24, and 1.67 H-25).

The presence of 1 primary methyl at δ_C 12.0/C-29 (δ_H 0.83, t, J = 7 Hz, H-29) and an additional 1 methylene at δ_C 25.5/C-28 (δ_H 1.15, t, J = 3.1 Hz, H-28) confirmed the chain moiety of the stigmastane skeleton. Moreover, the attachment of a hydroxyl at C-3 (δ_C 71.9) with a hydroxyl proton (δ_H 4.53) and another double bond pair at C-5 (δ_C 140.8)/C-6 (δ_C 121.8) afforded the

whole structure of **1**. A comparison of the NMR data of compound **1** with those in the literature revealed that it was nearly identical which enabled us to identify it as stigmast-5-ene, known as *β*-sitosterol, with the structure shown in **Figure 1** [44,45].

***In vitro* antibacterial and antifungal activity**

Using the Kirby-Bauer method, the potential antibacterial activity of *β*-sitosterol compound was evaluated by determining the zones of inhibition against *S. mutans*, *S. sanguinis*, and *C. albicans*. The antibacterial and antifungal data for *β*-sitosterol are presented in **Table 2**. According to the MIC value classification, concentrations ranging from 101 to 500 $\mu g \cdot mL^{-1}$ indicate strong antibacterial activity, whereas those ranging from 500 to 1000 $\mu g \cdot mL^{-1}$ denote moderate antibacterial activity, and MIC more than 1000 $\mu g \cdot mL^{-1}$ indicates weak antibacterial activity [46,47]. **Table 2** shows that *β*-sitosterol (**1**) was most active against *S. mutans*, with an MIC of 312.5 ± 0.16 $\mu g \cdot mL^{-1,}$ which falls into the strong category. However, *S. sanguinis* has moderate activity, with low bactericidal (MBC) ability. Compared with *S. sanguinis*, compound **1** also has moderate fungicidal ability against *C. albicans.* Therefore, it can be concluded that compound **1** has the strongest activity against *S. mutans.* This could be due to several factors, one of which is the different specificities of virulence factors in *S. mutans* and *S. sanguinis*, one of which is the biofilm-forming virulence enzyme expressed by *S. mutans*, which is highly dependent on glucose, so that if the compound is an inhibitor of the enzyme, the compound can disrupt the biofilm of *S. mutans* without affecting *S. sanguinis*, which does not depend on the gene or enzyme [48-50]. Therefore, the mechanism of the compound was predicted via *in silico* molecular docking to determine the interaction of the compound with key enzymes in *S. mutans*, *S. sanguinis*, and *C. albicans*, which cause pathogenicity [51].

Table 1 ^{1}H-NMR **(**700 MHz**)** and ^{13}C-NMR **(**175 MHz**)** data of compound 1 in $CDCl_3$ compared to the reference**.**

Carbon position	Compound 1 ($CDCl_3$)			*β*-sitosterol literature data ($CDCl_3$) [79,80]		
	δ_C (ppm) (175 MHz)	δ_H (ppm) (700 MHz)	DEPT	δ_C (ppm) (100 MHz)	δ_H (ppm) (400 MHz)	DEPT
C-1	37.3	1.85 (m, 2 H)	CH_2	37.4	1.85 (m, 2 H)	CH_2
C-2	31.7	1.95 (m, 2 H)	CH_2	31.8	1.95 (m, 2 H)	CH_2
C-3	71.9	3.52 (m, 1 H)	CH	72.0	3.55 (m, 1 H)	CH
C-4	42.2	2.30 (m, 2 H)	CH_2	42.4	2.38 (m, 2 H)	CH_2
C-5	140.8	-	C	140.9	-	C
C-6	121.8	5.36 (m, 1 H)	CH	121.9	5.37 (m, 1 H)	CH
C-7	31.9	1.99 (m, 2 H)	CH_2	32.1	1.99 (m, 2 H)	CH_2
C-8	31.9	2.02 (m, 1 H)	CH	31.9	2.00 (m, 1 H)	CH
C-9	50.2	0.95 (m, 1 H)	CH	50.3	0.94 (m, 1 H)	CH
C-10	36.6	-	C	36.6		C
C-11	21.2	1.02 (m, 2 H)	CH_2	21.2	1.02 (m, 2 H)	CH_2
C-12	39.8	1.16 (m, 2 H)	CH_2	39.9	1.16 (m, 2 H)	CH_2
C-13	42.4	-	C	42.5	-	C

Carbon position	Compound 1 ($CDCl_3$)			*β*-sitosterol literature data ($CDCl_3$) [79,80]		
	δ_C (ppm) (175 MHz)	**δ_H (ppm) (700 MHz)**	**DEPT**	**δ_C (ppm) (100 MHz)**	**δ_H (ppm) (400 MHz)**	**DEPT**
C-14	56	1.01 (m, 1 H)	CH	56.9	1.00 (m, 1 H)	CH
C-15	24.4	1.58 (m, 2 H)	CH_2	28.4	1.58 (m, 2 H)	CH_2
C-16	28.3	1.09 (m, 2 H)	CH_2	28.4	1.09 (m, 2 H)	CH_2
C-17	56.1	1.14 (m, 1 H)	CH	56.2	1.12 (m, 1 H)	CH
C-18	11.9	0.84 (s, 3 H)	CH_3	12.1	0.85 (s, 3 H)	CH_3
C-19	19.1	0.82 (s, 3 H)	CH_3	19.4	0.82 (s, 3 H)	CH_3
C-20	36.2	1.35 (m, 1 H)	CH	36.3	1.35 (m, 1 H)	CH
C-21	18.9	0.92 (d, J = 5.12 Hz, 3H)	CH_3	18.9	0.95 (d, 3 H)	CH_3
C-22	33.9	1.34 (m, 2 H)	CH_2	34.0	1.33 (m, 2 H)	CH_2
C-23	26.1	1.16 (m, 2 H)	CH_2	26.1	1.16 (m, 2 H)	CH_2
C-24	45.9	0.94 (m, 1 H)	CH	45.9	0.94 (m, 1 H)	CH
C-25	29.2	1.67 (m, 1 H)	CH	28.9	1.66 (m, 1 H)	CH
C-26	21.3	0.83 (d, J = 11 Hz, 3H)	CH_3	21.4	0,83 (d, 3 H)	CH_3
C-27	19.5	0.83 (d, 3 H)	CH_3	19.2	0.84 (d, 3 H)	CH_3
C-28	23.1	1.25 (m, 2 H)	CH_2	23.2	1.25 (m, 2 H)	CH_2
C-29	12.0	0.83 (m, 3 H)	CH_3	12.1	0.85 (m, 3 H)	CH_3

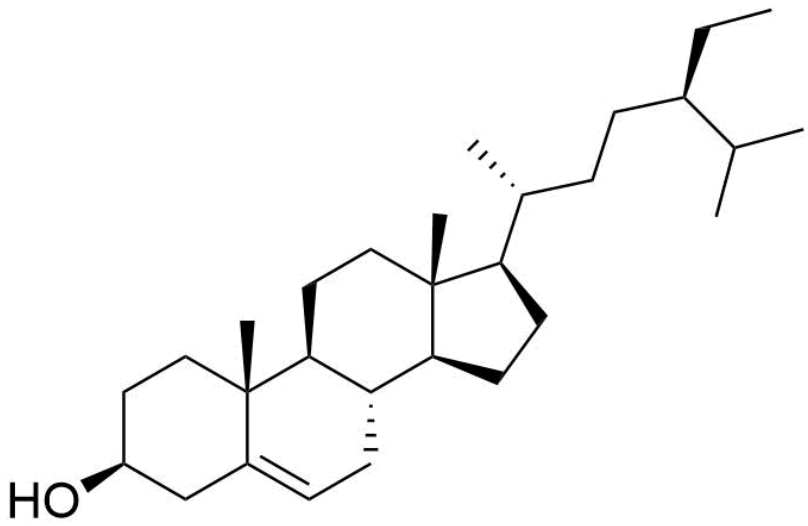

Figure 1 Structure of *β*-sitosterol (1).

Table 2 Antibacterial and antifungal activity of compound 1 (*in vitro*).

Organisms	Activity of compound 1		
	Inhibition zone at 2% (mm)	MIC (μg·mL^{-1})	MBC/MFC (μg·mL^{-1})
S. mutans	12.7 ± 0.84	312.5 ± 0.16	1250
S. sanguinis	10.63 ± 0.62	625 ± 0.11	2500
C. albicans	9.8 ± 0.75	625 ± 0.15	1250

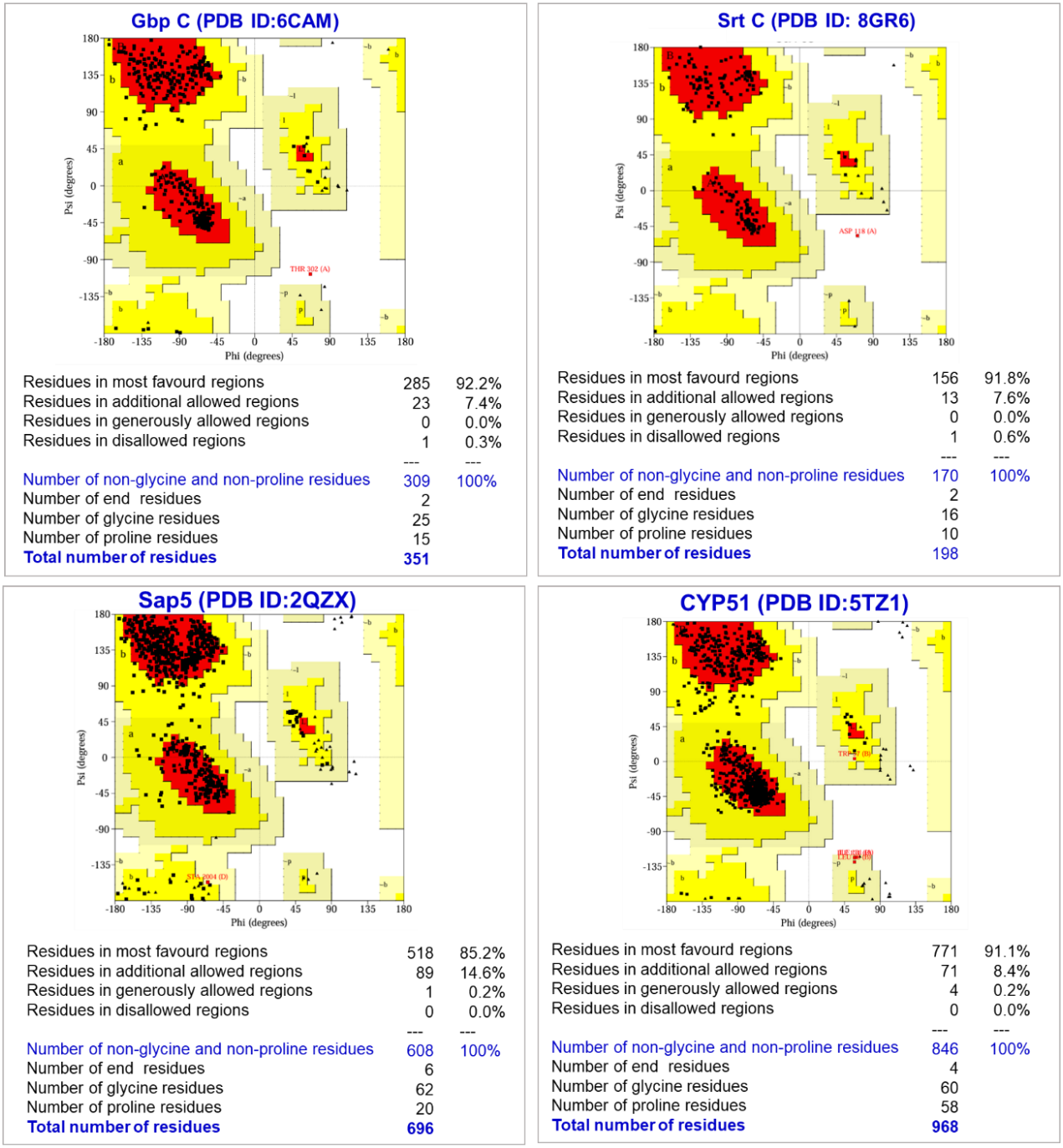

Figure 2 Ramachandran plot of GbpC, SrtC, Sap5, and CYP51 enzymes.

Ramachandran plot

Validation via the Ramachandran plot is a critical step for validating protein structures before molecular docking studies to ensure the reliability of the conformational data used in simulations. Ramachandran plot visualizing the backbone dihedral angles [52]. These angles determine how the peptide backbone folds and whether the conformation is sterically allowed. The favored regions are the most energetically favorable conformations with minimal steric clashes, namely the β-sheet area in the range $-180 < \varphi < -45$ and $45 < \psi < 225$ and the alpha-helix area in the range $-180 < \varphi < 0$ and $-100 < \psi < 45$ as the additional allowed region, the generously allowed regions in the range $0 < \varphi < 180$ and $-90 < \psi < 90$, and disallowed regions that are highly unfavorable due to steric clashes between atoms. The stereochemistry of the enzyme could be validated if there were not more than 2% amino acids in the generously allowed region [53,54].

As shown in **Figure 2**, the most favored regions, additionally allowed regions, generously allowed regions, and disallowed regions of Gbp C amino acid residues, were 92.2% (285), 7.4% (23), 0%, and 0.3% (**1**), respectively. In SrtC, the percentages were 91.8% (156), 7.6% (13), 0%, and 0.6% (1), respectively. The analysis revealed that the amino acid ASP 118 is situated in the disallowed region, indicating that this amino acid is not permitted in the active site area while docking. In Sap 5, the percentages were 85.2% (518), 14.6% (89), 0.2% (1), and 0%. In CYP51, there were 91.1% (771), 8.4% (71), 0.5% (4), and 0%, respectively. The percentage of these residues indicated that the stereochemistry of the 4 enzymes could be well validated.

Molecular docking study

The inhibitory activity of the enzyme against β-sitosterol was monitored by comparing the binding affinity values of the molecular docking results against various key enzymes derived from *S. mutans*, *S. sanguinis*, and *C. albicans*, which play a role in biofilm formation that causes dental caries and oral diseases. This method allows the identification of the binding affinity and inhibitory potential of compounds against enzymes that play a role in biofilm formation. The docking results show low binding energy and stable interactions at the active site of the enzyme [55]. Therefore, this compound has potential as a specific inhibitor of the enzyme. The key enzymes targeted in the antibacterial *in silico* assay were GbpC (glucan-binding protein C) and SrtC (sortase C), whereas in the antifungal assay, the enzymes Sap5 (secreted aspartyl protease 5) and lanosterol-14-α-demethylase were targeted.

In addition to molecular docking tests with various targets involving β-sitosterol, docking was also conducted with β-sitosterol-derived compounds that differ in terms of a single functional group and have previously been isolated from natural materials. This was done to investigate how structural modifications in these derivative compounds influence the binding affinity to the enzyme target. By comparing the binding energy and interactions formed, it can be seen whether the presence of certain functional groups or structural changes can increase or decrease the inhibitor activity. In this study, the 3 β-sitosterol derivative compounds shown in **Figure 3** were selected, namely, stigmastanol (**2**), which is different from hydrogenated derivatives with saturated C5-C6 bonds (without Δ^5) [56]. β-sitosterol-3-O-glucoside (**3**) is a modification of the β-D-glucopyranoside group at the C-3 hydroxyl position of the sterol backbone [57,58], and compound 7-β-hydroxysitosterol (**4**) has a different structure in addition to a hydroxyl group (-OH) at C-7 [59,60].

The results of the molecular docking of the β-sitosterol compounds against the 4 enzymes shown in **Figure 4** and **Table 3** indicate that, as antibacterial agents, β-sitosterol is more potent at inhibiting the GbpC enzyme of *S. mutans* than the SrtC enzyme in *S. sanguinis*. This finding is in line with the *in vitro* test in which compound **1** more strongly inhibited *S. mutans*. As an antifungal agent, β-sitosterol has a lower binding affinity when docked to the lanosterol 14-alpha demethylase enzyme (−12.38 kcal/mol) than to the Sap5 enzyme (−9.13 kcal/mol). It can be hypothesized that β-sitosterol compounds may act better as specific inhibitors of the CYP51 enzyme, which has a role in inhibiting the biosynthesis of ergosterol, leading to the loss of fungal membrane integrity and function, rather than as Sap5 inhibitor enzyme that target *C. albicans* virulence enzymes [61].

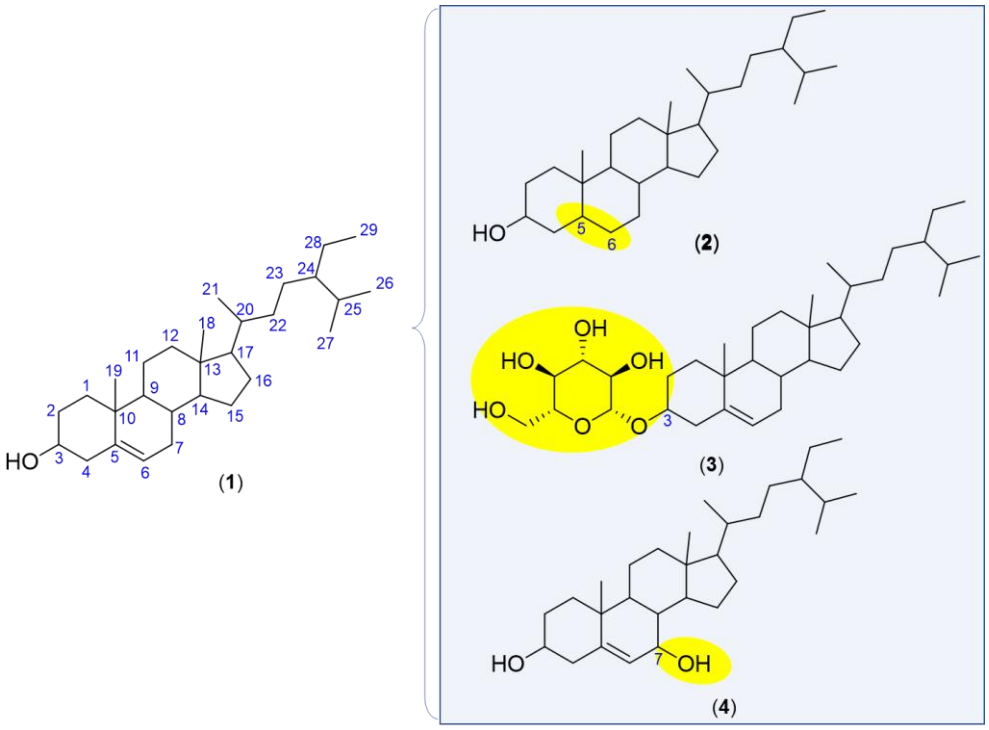

Figure 1 The structure of *β*-sitosterol and its derivatives, with the differences highlighted in yellow.

Table 2 Binding affinity of the complex protein-ligands.

Compounds	Compounds ID	Binding affinity (kcal/mol)				Inhibition constant (nM)			
		GbpC	SrtC	Sap5	CYP51	GbpC	SrtC	Sap5	CYP51
β-sitosterol (**1**)	222284	–9.91	–7.02	–9.13	–12.38	54.73	33210	201.61	0.8358
Stigmastanol (**2**)	241572	–9.11	–6.94	–9.77	–11.34	210.74	8210	69.3	4.87
β-sitosterol-3-O-*β*-d-glucoside (**3**)	12309057	–11.56	–7.66	–9.75	–13.15	3.38	5440	71.8	0.2306
7*β*-hydroxysitosterol (**4**)	12309569	–9.92	–6.65	–8.78	–12.05	53.63	13450	368.54	1.47

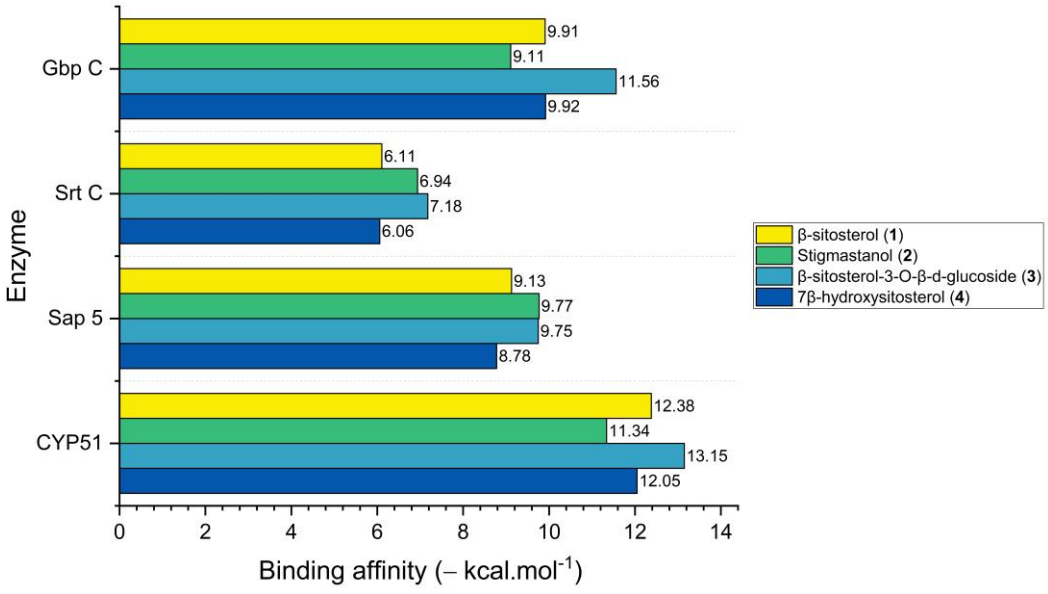

Figure 4 Binding affinity comparison of ***β*-**sitosterol and its derivatives against Gbp C, SrtC, Sap5, and CYP51.

In the Gbp C enzyme shown in **Figure 5**, compounds **1** and **2** have different types of interactions with the amino acid TRP:351. In compound 1, the interaction that occurs is only a pi-alkyl interaction, but in compound **2**, pi-alkyl and pi-sigma interactions occur. The difference from compound **3** is that more hydrogen interactions occur because it is clear from the glucoside structure that it has more OH functional groups than does compound **1**. The difference from compound **4** is that the addition of one -OH group at position C-7 has little effect, as it does not significantly increase the interaction with the enzyme active site, resulting in a minimal difference in bonding affinity.

In the Sap5 enzyme from *C. albicans*, as shown in **Figure 7**, compound 2 exhibited more hydrogen bond interactions than did compound 1, specifically at SER B:301 and ASP B:303, whereas compound 1 formed only 1 hydrogen bond with LYS B:193. Although compound **3** has fewer interactions, because hydrogen bonds are stronger and more stable than alkyl interactions are, it still has a strong bond affinity. In contrast, in compound **4**, the addition of OH groups reduces the interaction between the ligand and the enzyme due to the loss of hydrogen bonding interactions with the amino acid LYS B:193. The interaction of the ligand and lanosterol 14-alpha demethylase shown in **Figure 8** revealed that there were more interactions among all the compounds than among the other enzymes. This may be due to the match of the structure of *β*-sitosterol compounds and derivatives, which tend to be hydrophobic, with the active site contained in the enzyme.

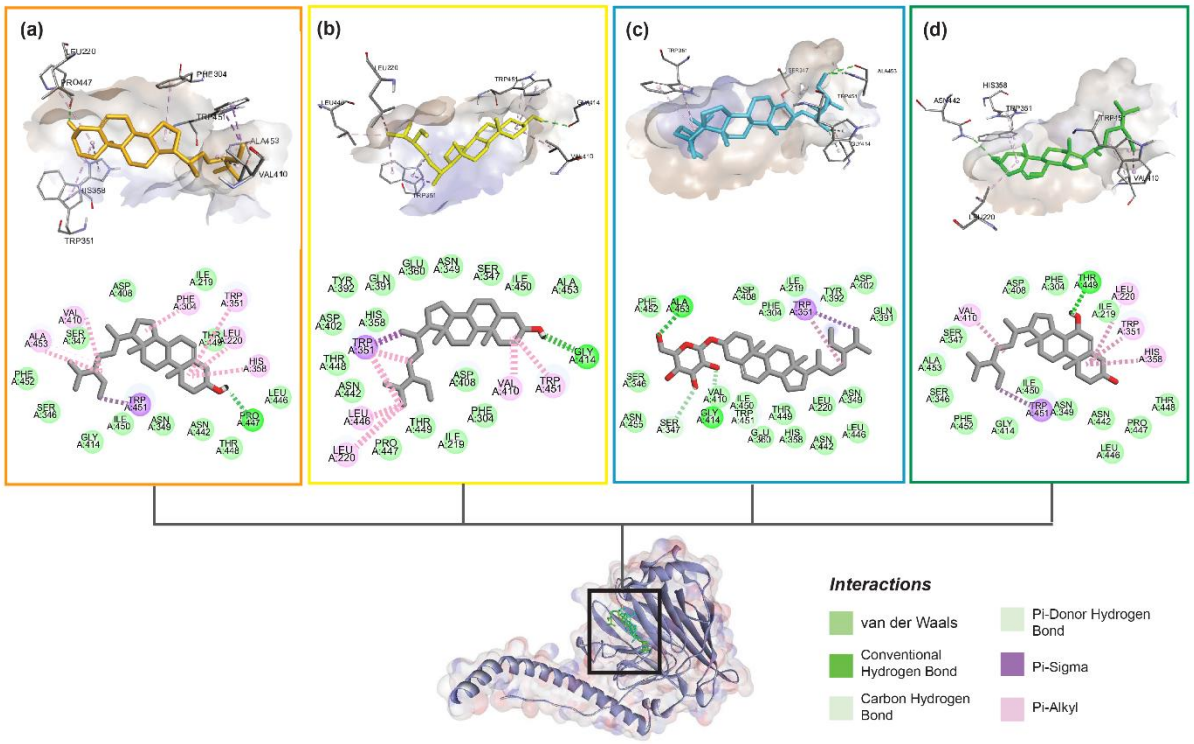

Figure 2 Molecular docking interactions from ***β*-**sitosterol **(**a**)** stigmastanol **(**b**)** *β*-sitosterol-3-O-***β*-**d-glucoside **(**c**)**, and 7***β*-**hydroxysitosterol **(**d**)** with the glucan binding protein C enzyme from *S. mutans*.

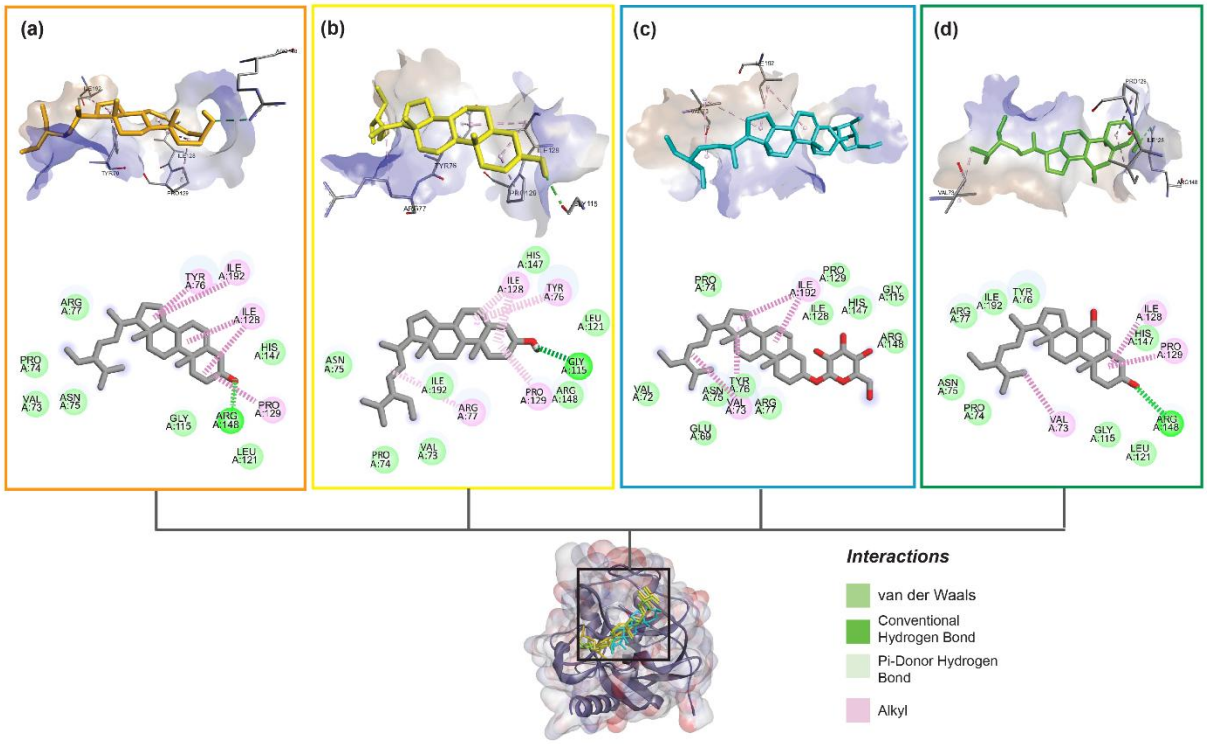

Figure 3 Molecular docking interactions from *β*-sitosterol **(**a**)**, stigmastanol **(**b**)**, *β*-sitosterol-3-O-*β*-d-glucoside **(**c**)**, and 7*β*-hydroxy sitosterol **(**d**)** with the sortase C enzyme from *S. sanguinis***.**

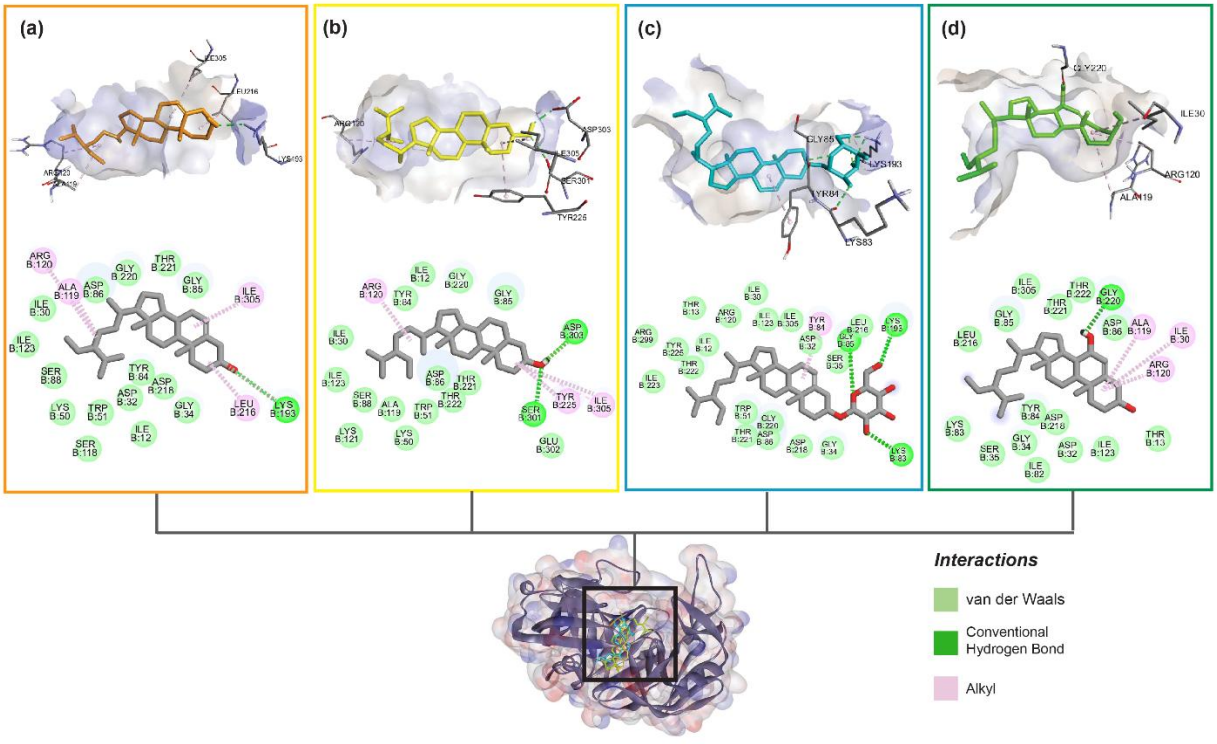

Figure 4 Molecular docking interactions from ***β***-sitosterol **(**a**)** stigmastanol **(**b**)** ***β***-sitosterol-3-O-***β***-d-glucoside **(**c**)** and 7***β***-hydroxy sitosterol **(**d**)** with secreted aspartyl protease 5 enzyme from *C. albicans***.**

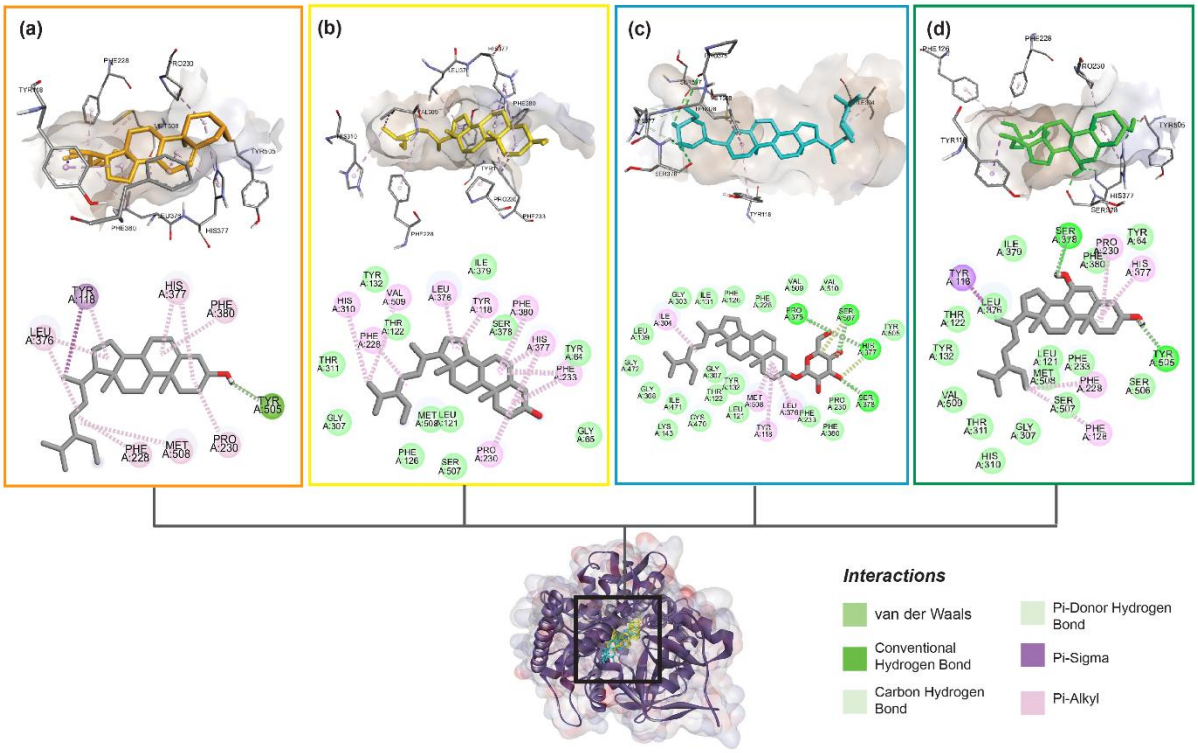

Figure 5 Molecular docking interactions from ***β***-sitosterol **(**a**)** stigmastanol **(**b**)** ***β***-sitosterol-3-O-***β***-d-glucoside **(**c**)** and 7***β***-hydroxy sitosterol **(**d**)** with lanosterol 14-alpha demethylase enzyme from *C. albicans***.**

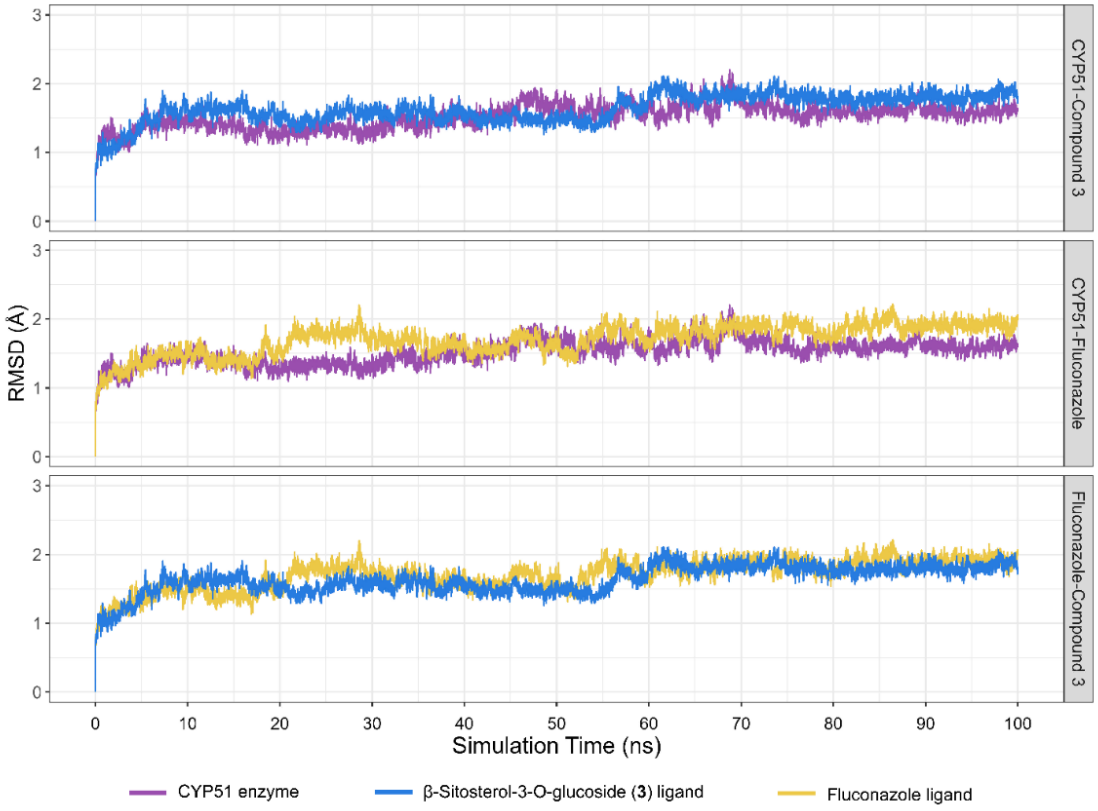

Figure 6 RMSD profiles of the CYP51 enzyme in complex with compound 3 and fluconazole as ligands.

Molecular dynamics simulation

To further validate the degree and stability of the binding between the compound and protein, this study conducted a 100 ns MD simulation [62]. Among the 5 enzyme-ligand complexes docking results, the complex between enzyme CYP51 and *β*-sitosterol-3-O-glucoside (**3**) was selected for MD simulation due to its more favorable binding free energy (−13.15 kcal.mol^{-1}) and stable docking conformation, suggesting a strong inhibitory potential. Fluconazole was used as a reference compound to compare the inhibitory potential of the test compound because it is a well-established commercial antifungal drug widely used to treat candidiasis [63]. Its antifungal activity is primarily due to the selective inhibition of the fungal enzyme lanosterol 14α-demethylase, a cytochrome P450 enzyme essential for ergosterol biosynthesis [64].

The RMSD (Root Mean Square Deviation) curve is a key metric in molecular dynamics simulations to evaluate protein-ligand complexes' stability and conformational behavior. A lower RMSD value reflects minimal structural deviations within the complex, indicating enhanced stability [65]. The RMSD of the complex CYP51 with compound **3** after 100 ns simulation with a mean value of 1.637 Å and a standard deviation of 0.202, indicating a stable interaction, as evidenced by an RMSD value of less than 3 Å [66]. **Figure 9** and **Table S3** shows that compound **3** exhibits a higher RMSD profile compared to the apo form of CYP51 enzyme, yet maintains a lower RMSD than fluconazole, a known CYP51 inhibitor. This result indicates a more stable and favorable complex formation between *β*-sitosterol-3-O-*β*-D-glucoside (**3**) and CYP51, highlighting its strong potential inhibitory activity against CYP51 in *C. albicans.*

The RMSF (Root Mean Square Fluctuation) analysis was conducted to evaluate the fluctuation of residues in the CYP51 enzyme during simulations, providing insights to the structural stability of the protein-ligand complexes. Lower values of RMSF indicate minimal movement, while higher RMSF values suggest larger fluctuations [67,68]. The RMSF curve for the compound 3 - CYP51 complex shows minor fluctuations, all within 1 nm, with no major deviations. **Figure 10** provides insight into the flexibility of amino acid residues within the CYP51 enzyme in the presence of different ligands. The comparison of notable differences in structural dynamics upon ligand binding. In the CYP51-fluconazole complex, several regions, particularly residues 220 - 250 and 390 - 420, exhibit increased fluctuations relative to the unbound enzyme, suggesting localized flexibility and potential conformational adaptation upon ligand interaction. These peaks are indicative of dynamic loop or surface regions responding to the steric and chemical nature of the ligand. In contrast, the CYP51-compound **3** complex shows a highly similar RMSF profile to the apo enzyme, with only minor increases in fluctuation in comparable regions. This implies that compound **3** induces minimal conformational changes and binds more stably, possibly due to stronger or more specific interactions with the active site.

The Molecular Mechanics Generalized Born Surface Area (MMGBSA) is an analytical approach to estimate the Gibbs binding free energy (ΔG) of a ligand to a receptor, indicating the strength of a ligand binding to its target [65]. **Figure 11** illustrates the molecular mechanics/generalized Born surface area (MM/GBSA) binding free energy (ΔG MMGBSA) for the CYP51 enzyme in complex with either compound **3** or fluconazole, measured over a series of 10-nanosecond sliding windows during molecular dynamics simulations. In this context, more negative values represent stronger binding affinity. Across all time windows, compound **3** consistently shows significantly more negative binding free energy values (approximately −80 to −100 kcal/mol), indicating a robust and stable interaction with CYP51 [69]. In contrast, fluconazole demonstrates less favourable binding energies, fluctuating between −20 and −40 kcal/mol, with more pronounced variability and larger error bars. This suggests that fluconazole forms a comparatively weaker and more dynamic interaction with the target enzyme. The stability of compound **3** binding energy over time further supports its tight and sustained binding, reinforcing its role as a highly effective CYP51 inhibitor.

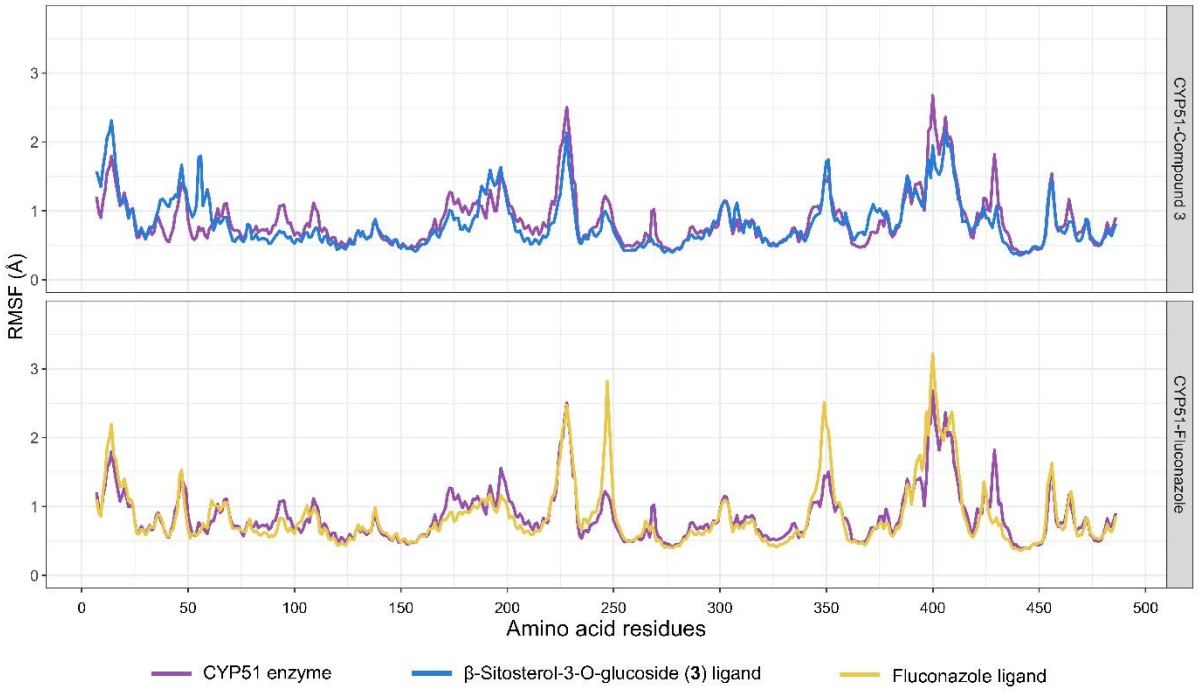

Figure 7 RMSF profiles of the CYP51 enzyme in complex with compound **3** and fluconazole.

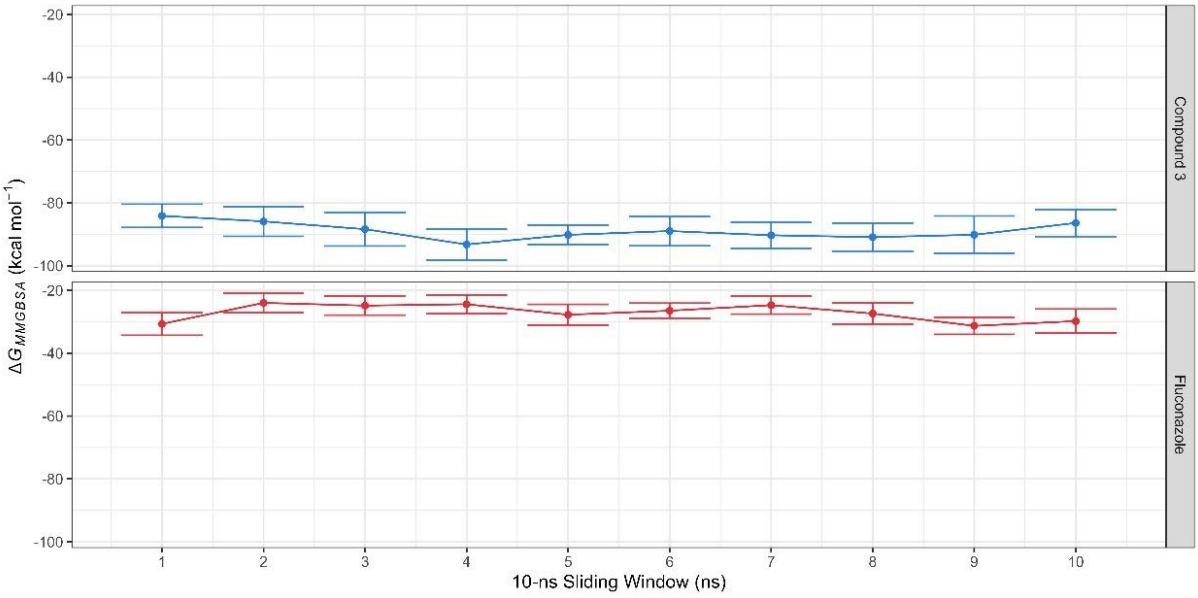

Figure 8 Time-dependent MM-GBSA binding free energy **(**ΔG °**)** profiles for compound 3 and fluconazole over a 100 ns molecular dynamics simulation, calculated using a 10-ns sliding window.

The hydrogen bond (H-bond) analysis shown in **Figure 12** offers further insights into the binding stability of the CYP51-ligand complexes observed during the 100 ns molecular dynamics simulation [70]. Compound **3** forms a relatively high and sustained number of hydrogen bonds with CYP51, ranging mostly between 2 and 4 throughout the simulation. This frequent hydrogen bonding indicates dynamic but consistent interaction with the binding site, possibly reflecting the ligand's adaptability to the binding pocket [70]. In contrast, fluconazole forms fewer hydrogen bonds, generally maintaining between 0 and 2 over the same simulation period. This confirms the MMGBSA analysis results that the Gibbs energy value of

compound **3** is smaller than fluconazole. Thus, the combined data suggest that compound **3** relies heavily on hydrogen bonding for stability and molecular interactions.

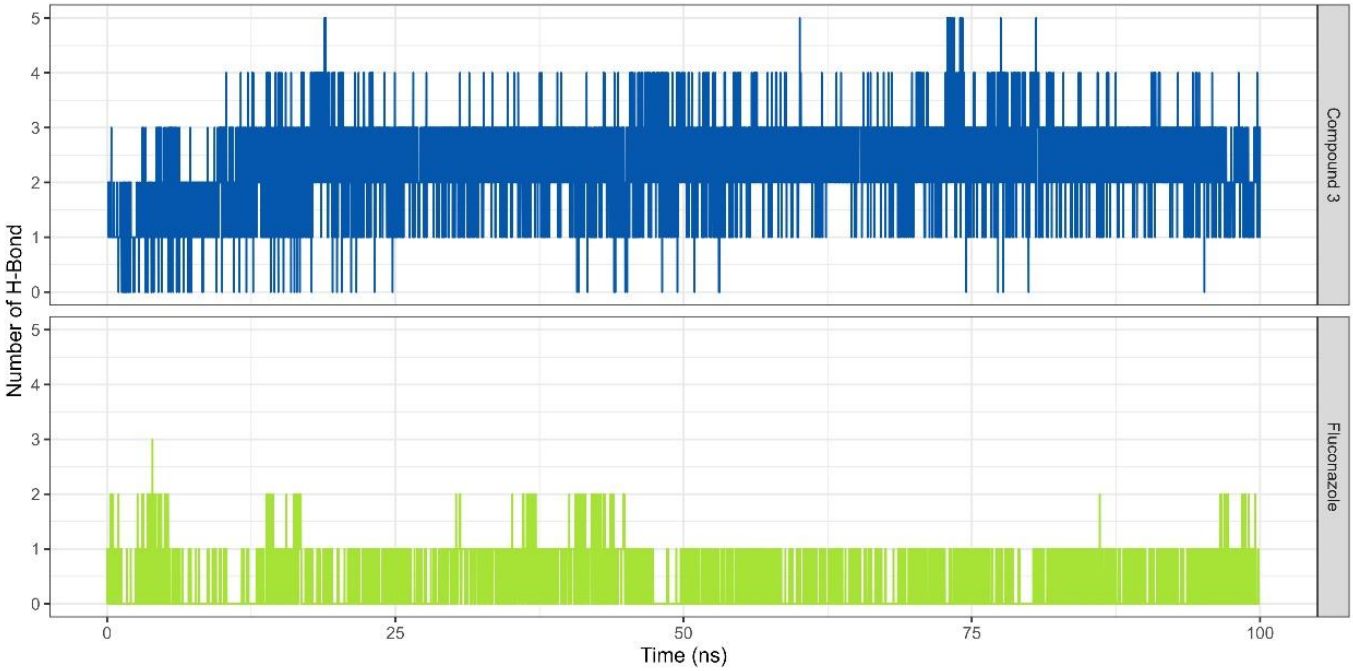

Figure 12 Number of hydrogen bonds formed over a 100 nm MD between CYP51 with compound 3 and fluconazole.

ADMET and drug-likeness analysis

Pharmacokinetic characteristics related to absorption, distribution, metabolism, excretion, and toxicity often lead to compounds failing in clinical trials [71]. Consequently, performing *in silico* experiments to evaluate various parameters of compounds is essential [72]. The water solubility for the absorption parameter is assessed on a scale from −5 to 0, with intestinal absorption considered adequate if it exceeds 80%. Compounds **1**, **2**, **3** and **4** were shown to have very low aqueous solubility values but high intestinal absorption, as shown in **Figure 9**. This combination of low solubility and high absorption suggests that these compounds could be effective drugs despite their solubility challenges, provided that appropriate formulation strategies are employed to ensure consistent bioavailability [73].

In terms of distribution, a logVDss value of −0.15 or lower signifies a low distribution, whereas values exceeding 0.45 indicate a high distribution. **Table 4** shows that all the compounds are poorly distributed [74]. Drugs with a low volume of distribution (Vdss) tend to remain primarily in the plasma, which implies that a lower dose is required to reach the desired plasma concentration.

Furthermore, absorption across the blood-brain barrier (BBB) and into the central nervous system (CNS) is classified as high if it exceeds 0.2, moderate if it falls between 0.1 and 0.2, and weak if it is less than 0.1. Compounds **1**, **2**, **3**, and **4** had CNS permeability values less than 0.1 (low), except for compound 1, which had a high BBB permeability value above 0.781.

Cytochrome P450 enzymes (CYP enzymes) are crucial in human drug metabolism. In this study, antimicrobial compounds that target bacteria and fungi specifically and do not involve human CYP enzymes were sought. Thus, the main therapeutic goal of antimicrobials is to eliminate or reduce pathogenicity without harming the host. Inhibiting CYP enzymes does not support this goal and may affect treatment by affecting the metabolism of other drugs and potentially causing toxicity [75]. All the test compounds were predicted not to be CYP inhibitors that interfere with human metabolism. Therefore, compounds **1**, **2**, **3**, and **4** have good potential.

The total clearance (CL) measures the total volume of plasma removed by the drug per unit time and is

expressed in units such as mL/min or L/h. In the evaluation of drugs, toxicity plays a crucial role. The classification of compounds based on their LD50 values, ranging from nontoxic (LD50 > 5000 mg/kg) to highly fatal (LD50 < 5 mg/kg), serves as a key framework for evaluating the potential toxicity of substances [76].

Table 5 shows that a bioavailability score of 0.55 indicates that approximately 55% of the administered dose of a drug reaches the systemic circulation in its active form. While some drugs are absorbed effectively, there is room for improvement through formulation or dosing adjustments to increase therapeutic efficacy [77]. Drugs with low bioavailability may require higher doses to achieve therapeutic levels when used in oral administration systems, which can increase the risk of side effects. Efforts might focus on improving solubility, using solubilizing agents or designing formulations that bypass first-pass metabolism.

Table 3 ADMET prediction of ***β*-sitosterol** and its derivative compounds**.**

Properties	Parameters	Predicted value			
		***β*-sitosterol (1)**	**Stigmastanol (2)**	***β*-sitosterol-3-O-*β*-d-glucoside (3)**	**7*β*-Hydroxysitosterol (4)**
Absorption	Water solubility (log mol/L)	–6.773	–6.063	–4.741	–6.249
	Intestinal Absorption (% absorbed)	94.464	94.938	79.677	94.737
	Skin Permeability	–2.783	–2.737	–2.748	–2.864
Distribution	Volume Distribution (VDss, log L/kg)	0.193	–0.108	–1.163	–0.087
	BBB Permeability (log BBB)	0.78	0.813	–0.78	–0.12
	CNS Permeability (log PS)	–1.705	–1.435	–3.021	–1.887
Metabolism	CYP1A2	No	No	No	No
	CYP2C19	No	No	No	No
	Inhibitor of: CYP2C9	No	No	No	No
	CYP2D6	No	No	No	No
	CYP3A4	No	No	No	No
Excretion	Total Clearance (log ml/min/kg)	0.628	0.621	0.689	0.653
Toxicity	Lethal Dose 50 % (mg/kg)	2.552	2.783	2.571	2.804
	Skin sensitisation	No	No	No	No

Table 5 Physicochemical properties of *β*-sitosterol and its derivative compounds**.**

Physicochemical properties	Compounds			
	β-sitosterol (1)	**Stigmastanol (2)**	**β-sitosterol-3-O-β-d-glucoside (3)**	**7β-Hydroxysitosterol (4)**
Chemical Formula	$C_{29}H_{50}O$	$C_{29}H_{52}O$	$C_{35}H_{60}O_6$	$C_{29}H_{50}O_2$
Molecular mass (≤500 g/mol)	414.39 g/mol	416.40 g/mol	576.44 g/mol	430.38 g/mol
Hydrogen bond acceptor (≤10)	1	1	6	2
Hydrogen bond donor (<5)	1	1	4	2
Molar refractivity (130≥ MR index ≥40)	133.23	133.70	165.61	134.39
Number of heteroatom (1 ~ 15)	1	1	6	2
Number of rigid bonds (0 ~ 30)	20	20	26	20
Formal charge (–4 ~ 4)	0	0	0	0
Lipophilicity				
Log $P_{o/w}$ (iLOGP)	5.05	5.17	5.15	4.81
Log $P_{o/w}$ (XLOGP3)	9.34	8.32	7.74	8.23
Log $P_{o/w}$ (WLOGP)	8.02	8.10	5.85	7
Log $P_{o/w}$ (MLOGP)	6.73	6.88	3.96	5.8

Physicochemical properties	Compounds			
	β-sitosterol (1)	**Stigmastanol (2)**	**β-sitosterol-3-O-β-d-glucoside (3)**	**7β-Hydroxysitosterol (4)**
Log $P_{o/w}$ (SILICOS-IT)	7.04	7.05	5.02	6.15
Druglikeness				
Lipinski	Yes; 1 violation: MLOGP > 4.15	Yes; 1 violation: MLOGP > 4.15	Yes; 1 violation: MW > 500	Yes; 1 violation: MLOGP > 4.15
Ghose	No; 3 violations: WLOGP > 5.6, MR > 130	No; 3 violations: WLOGP > 5.6, MR > 130, #atoms > 70	No; 4 violations: MW > 480, WLOGP > 5.6, MR > 130, #atoms > 70	No; 3 violations: WLOGP > 5.6, MR > 130, #atoms > 70
Veber	Yes	Yes	Yes	Yes
Egan	No; 1 violation: WLOGP > 5.88	No; 1 violation: WLOGP > 5.88	Yes	No; 1 violation: WLOGP > 5.88
Muegge	No; 2 violations: XLOGP3 > 5, Heteroatoms < 2	No; 2 violations: XLOGP3 > 5, Heteroatoms < 2	No; 1 violation: XLOGP3 > 5	No; 1 violation: XLOGP3 > 5
Bioavailability score	0.55	0.55	0.55	0.55

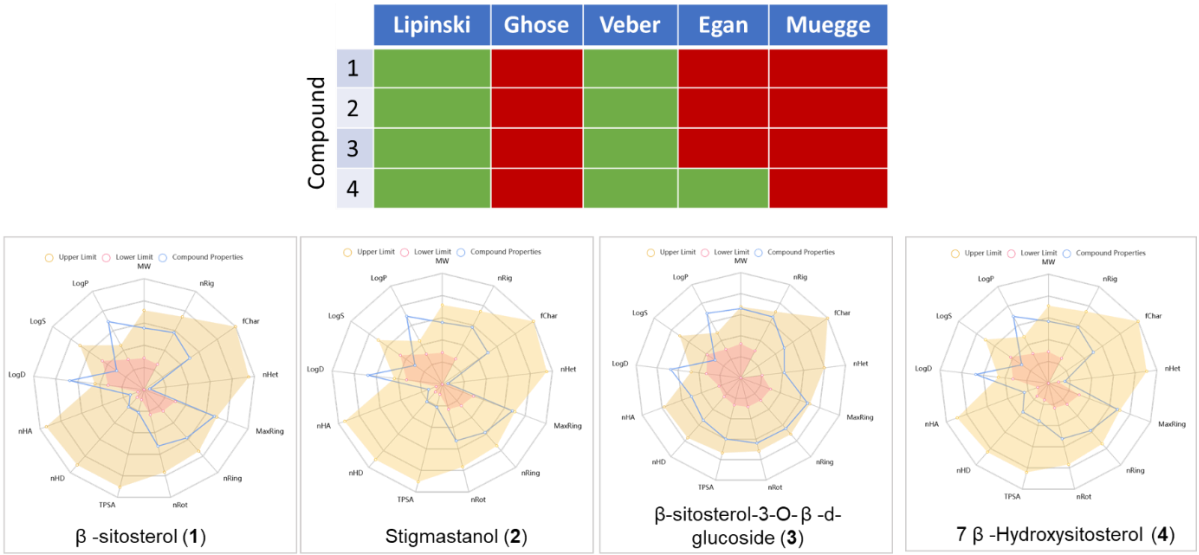

Figure 9 ADMETlab bioavailability radar of different bioactive drug-likeness molecules, where the blue areas represent each property **(**lipophilicity, molecular weight, solubility, and flexibility**).**

According to the drug-likeness prediction results, all the compounds fulfill the Lipinski and Veber rules, but there are discrepancies with the Ghose and Egan rules, except for compound 3, which fulfills all the rules except for Ghose. Lipinski's rule of 5 ensures that the compound likely has favorable pharmacokinetics for oral bioavailability, whereas Veber's rule focuses on oral bioavailability through structural flexibility and polarity. The Ghose filter adds stricter criteria for molecular weight (180 - 480), logP (−0.4 to +5.6), molar refractivity (40 - 130), and atom count (20 - 70) [78]. Noncompliance could indicate issues with size, lipophilicity, or molecular complexity. Egan's rule evaluates drug permeability and solubility via logP and PSA. A failure here may suggest potential challenges with solubility or membrane permeability. Muegge's rule applies broader drug-likeness filters, including molecular weight, logP, H-bond donors/acceptors, and rotatable bonds. Noncompliance may indicate deviations from general drug-like profiles.

These compounds may still be orally bioavailable according to Lipinski and Veber. Still, they could face challenges in terms of solubility, permeability, or similarity to drugs as defined by Ghose, Egan, or Muegge. This highlights the need for further experimental validation of pharmacokinetic and

pharmacodynamic properties. Although the compliance of Lipinski and Veber indicates the potential for good oral bioavailability, noncompliance with Ghose, Egan, and Muegge may require additional scrutiny regarding their solubility and permeability.

Conclusions

β-sitosterol (**1**) has been isolated from the methanol extract of *P. crocatum* leaves, the 1st obtained from this species. β-sitosterol (**1**) showed antimicrobial activity against oral pathogenic microbes, *S. mutans*, *S. sanguinis*, and the fungus *C. albicans*. The inhibitory potential of β-sitosterol against the 3 microbes showed moderate results, and was highly potent against *S. mutans*. The *in silico* molecular docking study also showed potential results, which showed good binding affinity for the four potential targets as antibacterial and antifungal with a broad spectrum. The molecular docking results showed that β-sitosterol is very strong in inhibiting Gbp C enzyme for bacteria, and CYP51 for *C. albicans* fungi, which is characterized by the highest binding affinity value. β-sitosterol-3-O-β-d-glucoside (**3**) exhibited stronger activity across all enzyme docking tests due to increased hydrogen bonding, further supported by molecular dynamics simulations showing lower RMSD values, indicating greater structural stability. The results of drug-likeness analysis also showed quite promising results as an oral drug with several parameter considerations. Based on the *in vitro* and *in silico* results, it can be concluded that β-sitosterol and its derivatives have good potential as antimicrobials, especially against oral pathogenic microbes. However, further studies are needed to validate its efficacy through enzyme assays and *in vivo* experiments. Additionally, structural modification of the compound could be explored to improve its potential issues with solubility and permeability.

Acknowledgements

This study was supported by Outstanding Scholarship from the Ministry of Education, Culture, Research, and Technology, Indonesia, and the Academic Leadership Grant (ALG) Universitas Padjadjaran, Indonesia, under the leadership of Prof. Dikdik Kurnia, M.Sc., Ph.D.

Declaration of Generative AI in Scientific Writing

No generative AI or AI-assisted technologies were used in the writing of this manuscript.

CRediT Author Statement

Norma Aura Tristyaningrum: Conceptualization, Investigation, Visualization, Writing – original draft.

Tati Herlina: Data curation, Formal analysis, Supervision, Writing - Review & Editing.

Dikdik Kurnia: Validation, Resources, Project administration, Funding acquisition.

References

[1] P Natarajan, S Madanian and S Marshall. Investigating the link between oral health conditions and systemic diseases: A cross-sectional analysis. *Scientific Reports* 2025; **15**, 10476.

[2] B Zhu, LC Macleod, T Kitten and P Xu. *Streptococcus sanguinis* biofilm formation & interaction with oral pathogens. *Future Microbiology* 2018; **13(8)**, 915-932.

[3] SF Kane. The effects of oral health on systemic health. *General Dentistry* 2017; **65(6)**, 30-34.

[4] MS Tonetti, P Bottenberg, G Conrads, P Eickholz, P Heasman, MC Huysmans, R López, P Madianos, F Müller, I Needleman, B Nyvad, PM Preshaw, I Pretty, S Renvert, F Schwendicke, L Trombelli, GJVD Putten, J Vanobbergen, N West, A Young and S Paris. Dental caries and periodontal diseases in the ageing population: Call to action to protect and enhance oral health and well-being as an essential component of healthy ageing. *Journal of Clinical Periodontology* 2017; **44(S18)**, S135-S144.

[5] JH Meurman and A Bascones-Martinez. Oral infections and systemic health - More than just links to cardiovascular diseases. *Oral Health and Preventive Dentistry* 2021; **19**, 441-448.

[6] D Shetty, M Dua, K Kumar, R Dhanapal, M Astekar and DC Shetty. Oral hygiene status of individuals with cardiovascular diseases and associated risk factors. *Clinics and Practice* 2012; **2(4)**, e86.

[7] WJ Loesche. Role of *Streptococcus mutans* in human dental decay. *Microbiology Reviews* 1986; **50(4)**, 353-380.

[8] C Nabert-Georgi, AC Rodloff, H Jentsch, DR Reissmann, R Schaumann and CS Stingu. Influence of oral bacteria on adhesion of *Streptococcus mutans* and *Streptococcus sanguinis* to dental materials. *Clinical and Experimental Dental Research* 2018; **4(3)**, 72-77.

[9] CO Truss. The role of *Candida albicans* in human illness. *Journal of Orthomolecular Psychiatry* 1981; **10**, 228-238.

[10] M Patel. Oral cavity and *Candida albicans*: Colonisation to the development of infection. *Pathogens* 2022; **11(3)**, 335.

[11] S Patil, RS Rao, B Majumdar and S Anil. Clinical appearance of oral *Candida* infection and therapeutic strategies. *Frontiers in Microbiology* 2015; **6**, 1391.

[12] W Qiu, Y Zhou, Z Li, T Huang, Y Xiao, L Cheng, X Peng, L Zhang and B Ren. Application of antibiotics/antimicrobial agents on dental caries. *BioMed Research International* 2020; **2020**, 5658212.

[13] R Rautemaa and G Ramage. Oral candidosis-clinical challenges of a biofilm disease. *Critical Reviews in Microbiology* 2011; **37(4)**, 328-336.

[14] MC Fisher, A Alastruey-Izquierdo, J Berman, T Bicanic, EM Bignell, P Bowyer, M Bromley, R Brüggemann, G Garber, OA Cornely, SJ Gurr, TS Harrison, E Kuijper, J Rhodes, DC Sheppard, A Warris, PL White, J Xu, B Zwaan and PE Verweij. Tackling the emerging threat of antifungal resistance to human health. *Nature Reviews Microbiology* 2022; **20**, 557-571.

[15] A Arastehfar, T Gabaldón, R Garcia-Rubio, JD Jenks, M Hoenigl, HJF Salzer, M Ilkit, C Lass-Flörl and DS Perlin. Drug-resistant fungi: An emerging challenge threatening our limited antifungal armamentarium. *Antibiotics* 2020; **9(12)**, 877.

[16] MC Fisher, NJ Hawkins, D Sanglard and SJ Gurr. Worldwide emergence of resistance to antifungal drugs challenges human health and food security. *Science* 2018; **360(6390)**, 739-742.

[17] A Budimir. *Fighting antimicrobial resistance*. IAPC Publishing, Zagreb, Croatia, 2018.

[18] NA Church and JL McKillip. Antibiotic resistance crisis: Challenges and imperatives. *Biologia* 2021; **76**, 1535-1550.

[19] AN Olaimat, MA Al-Holy, HM Shahbaz, AA Al-Nabulsi, MHA Ghoush, TM Osaili, MM Ayyash and RA Holley. Emergence of antibiotic resistance in *Listeria monocytogenes* isolated from food products: A comprehensive review. *Comprehensive Reviews in Food Science and Food Safety* 2018; **17**, 1277-1292.

[20] AT Nishimoto, C Sharma and PD Rogers. Molecular and genetic basis of azole antifungal resistance in the opportunistic pathogenic fungus *Candida albicans*. *Journal of Antimicrobial Chemotherapy* 2020; **75(2)**, 257-270.

[21] S Silva, CF Rodrigues, D Araújo, ME Rodrigues and M Henriques. Candida species biofilms' antifungal resistance. *Journal of Fungi* 2017; **3(1)**, 8.

[22] SK Ahmed, S Hussein, K Qurbani, RH Ibrahim, A Fareeq, KA Mahmood and MG Mohamed. Antimicrobial resistance: Impacts, challenges, and future prospects. *Journal of Medicine, Surgery, and Public Health* 2024; **2**, 100081.

[23] Z Khan, N Nath, A Rauf, TB Emran, S Mitra, F Islam, D Chandran, J Barua, MU Khandaker, AM Idris, P Wilairatana and M Thiruvengadam. Multifunctional roles and pharmacological potential of β-sitosterol: Emerging evidence toward clinical applications. *Chemico-biological Interactions* 2022; **365**, 110117.

[24] R Barbieri, E Coppo, A Marchese, M Daglia, E Sobarzo-Sánchez, SF Nabavi and SM Nabavi. Phytochemicals for human disease: An update on plant-derived compounds antibacterial activity. *Microbiological Research* 2017; **196**, 44-68.

[25] D Ghosh, N Datta, D Banerjee, S Adhikary, S Banerjee and A De. *Current trends on phytochemicals toward herbal medicine development*. *In*: SC Izah, MC Ogwu and M Akram (Eds.). Herbal medicine phytochemistry: Applications and trends. Springer, Cham, Switzerlands, 2024.

[26] SA Zacchino, E Butassi, E Cordisco and LA Svetaz. Hybrid combinations containing natural products and antimicrobial drugs that interfere

with bacterial and fungal biofilms. *Phytomedicine* 2017; **37**, 14-26.

[27] M Matsumoto-Nakano. Role of *Streptococcus mutans* surface proteins for biofilm formation. *Japanese Dental Science Review* 2018; **54(1)**, 22-29.

[28] T Rezaei, B Mehramouz, P Gholizadeh, L Yousefi, K Ganbarov, R Ghotaslou, S Taghizadeh and HS Kafil. Factors associated with *Streptococcus mutans* pathogenicity in the oral cavity. *Biointerface Research in Applied Chemistry* 2023; **13(4)**, 368.

[29] MB Winter, EC Salcedo, MB Lohse, N Hartooni, M Gulati, H Sanchez, J Takagi, B Hube, DR Andes, AD Johnson, CS Craik and CJ Nobile. Global identification of biofilm-specific proteolysis in *Candida albicans*. *mBio* 2016; **7(5)**, e01514-16.

[30] A Nobbs and J Kreth. Genetics of *sanguinis* - Group streptococci in health and disease. *Microbiology Spectrum* 2019. https://doi.org/10.1128/microbiolspec.GPP3-0052-2018.

[31] D Kurnia, E Apriyanti, C Soraya and MH Satari. Antibacterial flavonoids against oral bacteria of enterococcus faecalis ATCC 29212 from Sarang Semut (Myrmecodia pendans) and its inhibitor activity against enzyme MurA. *Current Drug Discovery Technologies* 2019; **16**, 290-296.

[32] SA Putri, AAN Shadrina, E Julaeha and D Kurnia. Potential nevadensin from ocimum basilicum as antibacterial agent against *Streptococcus mutans*: *In vitro* and *in silico* studies. *Combinatorial Chemistry and High Throughput Screening* 2023; **26(9)**, 1746-1754.

[33] SA Putri, E Julaeha, N Kagawa and D Kurnia. Phenolic compounds from *Ocimum basilicum* revealed as antibacterial by experimental and computational screening-based studies against oral infections. *Journal of Chemistry* 2024; **2024**, 3696250.

[34] D Kurnia, GS Hutabarat, D Windaryanti, T Herlina, Y Herdiyati and MH Satari. Potential allylpyrocatechol derivatives as antibacterial agent against oral pathogen of *S. sanguinis* ATCC 10556 and as inhibitor of MurA enzymes: *In vitro* and *in silico* study. *Drug Design, Development and Therapy* 2020; **14**, 2977-2985.

[35] DO Oladejo, GO Oduselu, TM Dokunmu, I Isewon, J Oyelade, E Okafor, EE Iweala and E Adebiyi. *In silico* structure prediction, molecular docking, and dynamic simulation of *Plasmodium falciparum* AP2-I transcription factor. *Bioinformatics and Biology Insights* 2023; **17**, 11779322221149616.

[36] S Shaweta, S Akhil and G Utsav. Molecular docking studies on the Anti-fungal activity of *Allium sativum* (Garlic) against *Mucormycosis* (black fungus) by BIOVIA discovery studio visualizer 21.1.0.0. *Annals of Antivirals and Antiretrovirals* 2021; **2021**, 28-32.

[37] WP Feinstein and M Brylinski. Calculating an optimal box size for ligand docking and virtual screening against experimental and predicted binding pockets. *Journal of Cheminformatics* 2015; **7**, 18.

[38] E Mateev, I Valkova, B Angelov, M Georgieva and A Zlatkov. Validation through re-docking, cross-docking and ligand enrichment in various well-resoluted MAO-B receptors. *International Journal of Pharmaceutical Sciences and Research* 2022; **13(8)**, 1099-1107.

[39] R Amini, S Moradi, R Najafi, M Mazdeh and A Taherkhani. BACE1 inhibition utilizing organic compounds holds promise as a potential treatment for Alzheimer's and Parkinson's diseases. *Oxidative Medicine and Cellular Longevity* 2024; **2024**, 6654606.

[40] FX Domínguez-Villa, NA Durán-Iturbide and JG Ávila-Zárraga. Synthesis, molecular docking, and *in silico* ADME/Tox profiling studies of new 1-aryl-5-(3-azidopropyl)indol-4-ones: Potential inhibitors of SARS CoV-2 main protease. *Bioorganic Chemistry* 2021; **106**, 104497.

[41] PV Zadorozhnii, VV Kiselev and AV Kharchenko. *In slico* ADME profiling of salubrinal and its analogues. *Future Pharmacology* 2022; **2(2)**, 160-197.

[42] U Das, T Chanda, J Kumar and A Peter. Discovery of natural MCL1 inhibitors using pharmacophore modelling, QSAR, docking, ADMET, molecular dynamics, and DFT analysis. *Computational Biology and Chemistry* 2025; **117**, 108427.

[43] L Fu, S Shi, J Yi, N Wang, Y He, Z Wu, J Peng, Y Deng, W Wang, C Wu, A Lyu, X Zeng, W Zhao, T Hou and D Cao. ADMETlab 3.0: An updated comprehensive online ADMET prediction platform enhanced with broader coverage, improved performance, API functionality and decision support. *Nucleic Acids Research* 2024; **52(W1)**, W422-W431.

[44] AJ Uttu, MS Sallau, H Ibrahim and ORA Iyun. Isolation, characterization, and docking studies of campesterol and β-sitosterol from *Strychnos innocua* (Delile) root bark. *Journal of Taibah University Medical Sciences* 2023; **18(3)**, 566-578.

[45] L Narayanan, T Maruthavanan, Vaithiyanathan R, G Venkatesan, KE Vivekanandan, G Kaliyannan, PSM Kumar, MSAJ Bosco, G Murugadoss and SR Suseem. Comprehensive investigation of antibacterial, cytotoxic, and antioxidant activities of *Ipomoea staphylina* flower extract with isolation and characterization of beta-sitosterol. *Journal of Molecular Structure* 2025; **1336**, 142045.

[46] L Cartuche, C Vallejo, E Castillo, N Cumbicus and V Morocho. Chemical profiling of *Drimys granadensis* (Winteraceae) essential oil, and their antimicrobial, antioxidant, and anticholinesterase properties. *Plants* 2024; **13(13)**, 1806.

[47] D Somda, JL Bargul, JM Wesonga and SW Wachira. Green synthesis of *Brassica carinata* microgreen silver nanoparticles, characterization, safety assessment, and antimicrobial activities. *Scientific Reports* 2024; **14**, 29273.

[48] K Rainey, SM Michalek, ZT Wen and H Wu. Glycosyltransferase-mediated biofilm matrix dynamics and virulence of *Streptococcus mutans*. *Applied and Environmental Microbiology* 2019; **85**, e02247-18.

[49] AM Martini, BS Moricz, AK Ripperger, PM Tran, ME Sharp, AN Forsythe, K Kulhankova, W Salgado-Pabón and BD Jones. Association of novel *Streptococcus sanguinis* virulence factors with pathogenesis in a native valve infective endocarditis model. *Frontiers in Microbiology* 2020; **11**, 10.

[50] B Nijampatnam, P Ahirwar, P Pukkanasut, H Womack, L Casals, H Zhang, X Cai, SM Michalek, H Wu and SE Velu. Discovery of potent inhibitors of *Streptococcus mutans* biofilm with antivirulence activity. *ACS Medicinal Chemistry Letters* 2021; **12(1)**, 48-55.

[51] TM Vieira, JG Barco, SLD Souza, ALO Santos, I Daoud, S Rahali, N Amdouni, JK Bastos, CHG Martins, RB Said and AEM Crotti. *In vitro* and *in silico* studies of the antimicrobial activity of prenylated phenylpropanoids of green propolis and their derivatives against oral bacteria. *Antibiotics* 2024; **13(8)**, 787.

[52] B Udosen, O Soremekun, C Ekenna, OI Omotuyi, T Chikowore, O Nashiru and S Fatumo. *In-silico* analysis reveals druggable single nucleotide polymorphisms in angiotensin 1 converting enzyme involved in the onset of blood pressure. *BMC Research Notes* 2021; **14**, 457.

[53] SC Lovell, IW Davis, WB Arendall, PIWD Bakker, JM Word, MG Prisant, JS Richardson and DC Richardson. Structure validation by Cα geometry: ϕ, ψ and Cβ deviation. *Proteins: Structure, Function, and Bioinformatics* 2003; **50(3)**, 437-450.

[54] GN Ramachandran, C Ramakrishnan and V Sasisekharan. Stereochemistry of polypeptide chain configurations. *Journal of Molecular Biology*. 1963; **7**, 95-99.

[55] A Abdullaev, I Abdullaev, A Bogbekov, U Gayibov, S Omonturdiev, S Gayibova, M Turahodjayev, K Ruziboev and T Aripov. Antioxidant potential of *Rhodiola heterodonta* extract: Activation of Nrf2 pathway via integrative *in vivo* and *in silico* studies. *Trends in Sciences* 2025; **22(5)**, 9521.

[56] OJ Juvik, B Holmelid, GW Francis, HL Andersen, APD Oliveira, RDGO Júnior, JGDS Almeida and T Fossen. Non-polar natural products from *Bromelia laciniosa*, *Neoglaziovia variegata* and *Encholirium spectabile* (Bromeliaceae). *Molecules* 2017; **22**, 1478.

[57] NS Njinga, MI Sule, UU Pateh, HS Hassan, ST Abdullahi and RN Ache. Isolation and antimicrobial activity of β-sitosterol-3-O-glucoside from *Lannea Kerstingii* Engl. & K. Krause (Anacardiacea). *Nitte University Journal of Health Sciences* 2016; **6(1)**, 4-8.

[58] T Peshin and HK Kar. Isolation and characterization of β-Sitosterol-3-O-β-D-glucoside from the extract of the flowers of *Viola odorata*. *British Journal of Pharmaceutical Research*. 2017; **16(4)**, 33160.

[59] N Tripathi, S Kumar and R Singh. Isolation of 7-β-Hydroxy-β-Sitosterol from roots of *Girardinia heterophylla* (Decne). *Asian Journal of Research in Chemistry* 2013; **6**, 1107-1109.

[60] D Labaree, RM Hoyte and RB Hochberg. A direct stereoselective synthesis of 7β-hydroxytestosterone. *Steroids* 1997; **62(6)**, 482-486.

[61] P Mohana, A Singh, F Rashid, S Singh, K Kaur, R Rana, PMS Bedi, N Bedi, R Kaur and S Arora. Inhibition of virulence associated traits by β-Sitosterol isolated from *Hibiscus rosa-sinensis* flowers against *Candida albicans*: Mechanistic insight and molecular docking studies. *Journal of Microbiology* 2024; **62(12)**, 1165-1175.

[62] J Wu, Y Zhou, J Zhang, HX Zhang and R Jia. Molecular dynamics simulation investigation of the binding and interaction of the EphA6-Odin protein complex. *The Journal of Physical Chemistry B* 2022; **126**, 4914-4924.

[63] PG Pappas, CA Kauffman, DR Andes, CJ Clancy, KA Marr, L Ostrosky-Zeichner, AC Reboli, MG Schuster, JA Vazquez, TJ Walsh, TE Zaoutis and JD Sobel. Clinical practice guideline for the management of candidiasis: 2016 update by the Infectious Diseases Society of America. *Clinical Infectious Diseases* 2016; **62(4)**, e1-e50.

[64] Y Feng, H Lu, M Whiteway and Y Jiang. Understanding fluconazole tolerance in *Candida albicans*: Implications for effective treatment of candidiasis and combating invasive fungal infections. *Journal of Global Antimicrobial Resistance* 2023; **35**, 314-321.

[65] T Herlina, V Nishinarizki, AWR Akili, A Hardianto, S Gaffar, M Muchtaridi and J Latip. Exploring *Erythrina* flavonoids as potential SARS-CoV-2 RdRp inhibitors through virtual screening, *in silico* ADMET evaluation, and molecular dynamics simulation studies. *Scientific Reports* 2025; **15**, 14259.

[66] JF Fatriansyah, AG Boanerges, SR Kurnianto, AF Pradana, Fadilah and SN Surip. Molecular dynamics simulation of ligands from *Anredera cordifolia* (Binahong) to the main protease (Mpro) of SARS-CoV-2. *Journal of Tropical Medicine* 2022; **2022**, 1178228.

[67] S Lee, AR Wong, AWH Yang and A Hung. Interaction of compounds derived from the Chinese medicinal formula Huangqi Guizhi Wuwu Tang with stroke-related numbness and weakness targets: An *in-silico* docking and molecular dynamics study. *Computers in Biology and Medicine* 2022; **146**, 105568.

[68] F Talab, A Alam, Zainab, S Ullah, AA Elhenawy, SAA Shah, M Ali, SA Halim, A Khan, A Latif, A Al-Harrasi and M Ahmad. Novel hydrazone schiff's base derivatives of polyhydroquinoline: Synthesis, *in vitro* prolyl oligopeptidase inhibitory activity and their Molecular docking study. *Journal of Biomolecular Structure and Dynamics* 2024. https://doi.org/10.1080/07391102.2024.2319677.

[69] I Sama-ae, NC Pattaranggoon and A Tedasen. *In silico* prediction of antifungal compounds from natural sources towards Lanosterol 14-alpha demethylase (CYP51) using molecular docking and molecular dynamic simulation. *Journal of Molecular Graphics and Modelling* 2023; **121**, 108435.

[70] MA Hosen, YE Bakri, HM Rehman, HE Hashem, M Saki and SMA Kawsar. A computational investigation of galactopyranoside esters as antimicrobial agents through antiviral, molecular docking, molecular dynamics, pharmacokinetics, and bioactivity prediction. *Journal of Biomolecular Structure and Dynamics* 2024; **42(2)**, 1015-1030.

[71] SQ Pantaleão, PO Fernandes, JE Gonçalves, VG Maltarollo and KM Honorio. Recent advances in the prediction of pharmacokinetics properties in drug design studies: A review. *ChemMedChem* 2022; **17(1)**, e202100542.

[72] L Kumari, Y Choudhari, P Patel, GD Gupta, D Singh, JM Rosenholm, KK Bansal and BD Kurmi. Advancement in solubilization approaches: A step towards bioavailability enhancement of poorly soluble drugs. *Life* 2023; **13**, 1099.

[73] DV Bhalani, B Nutan, A Kumar and AKS Chandel. Bioavailability enhancement techniques

for poorly aqueous soluble drugs and therapeutics. *Biomedicines* 2022; **10(9)**, 2055.

[74] K Arumugam, K Chandran, A Zochedh, S Ansar, AB Sultan, YA Kumar and T Kathiresan. Pharmacoinformatics and quantum chemicals-based analysis of aromatic molecule decanal as a potent drug against breast cancer. *International Journal of Quantum Chemistry* 2024; **124(15)**, e27451.

[75] M Zhao, J Ma, M Li, Y Zhang, B Jiang, X Zhao, C Huai, L Shen, N Zhang, L He and S Qin. Cytochrome P450 enzymes and drug metabolism in humans. *International Journal of Molecular Sciences* 2021; **22**, 12808.

[76] YY Zhang, YF Huang, J Liang and H Zhou. Improved up-and-down procedure for acute toxicity measurement with reliable LD_{50} verified by typical toxic alkaloids and modified Karber method. *BMC Pharmacology and Toxicology* 2022; **23(1)**, 3.

[77] M Stielow, A Witczyńska, N Kubryń, Ł Fijałkowski, J Nowaczyk and A Nowaczyk. The bioavailability of drugs—The current state of knowledge. *Molecules* 2023; **28(24)**, 8038.

[78] ASA Wasidi, AS Hassan and AM Naglah. *In vitro* cytotoxicity and druglikeness of pyrazolines and pyridines bearing benzofuran moiety. *Journal of Applied Pharmaceutical Science* 2020; **10**, 142-148.

[79] MO Aliba, IG Ndukwe and H Ibrahim. Isolation and characterization of B-sitosterol from methanol extracts of the stem bark of large-leaved rock fig (*Ficus abutilifolia* Miq.). *Journal of Applied Sciences and Environmental Management* 2018; **22**, 1639.

[80] Erwin, WR Pusparohmana, RD Safitry, E Marliana, Usman and IW Kusuma. Isolation and characterization of stigmasterol and beta-sitosterol from wood bark extract of *Baccaurea macrocarpa* Miq. Mull. Arg. *Rasayan Journal of Chemistry* 2020; **13**, 2552-2558.

Supplementary Materials

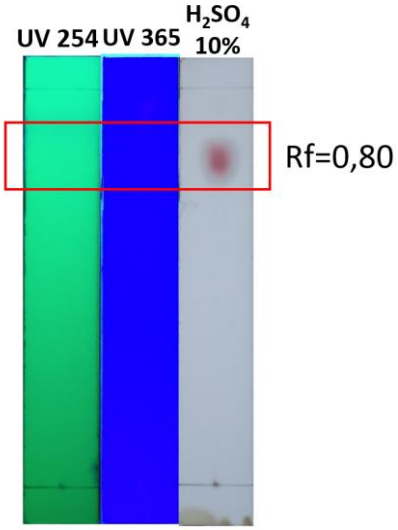

Figure S10 Thin layer chromatographic analysis of ***β***-Sitosterol
Stationary phase: Silica G 60 F_{254}
Mobile phase: *n*-hexane – ethyl acetate (4:6)

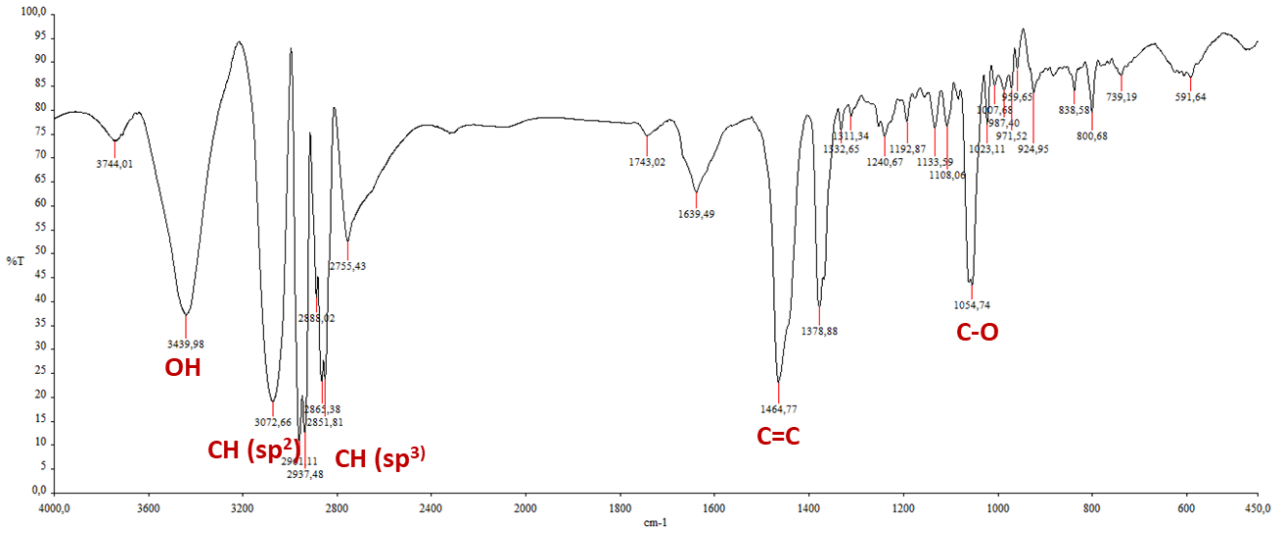

Figure S2 IR spectrum from Compound **1** (in KBr).

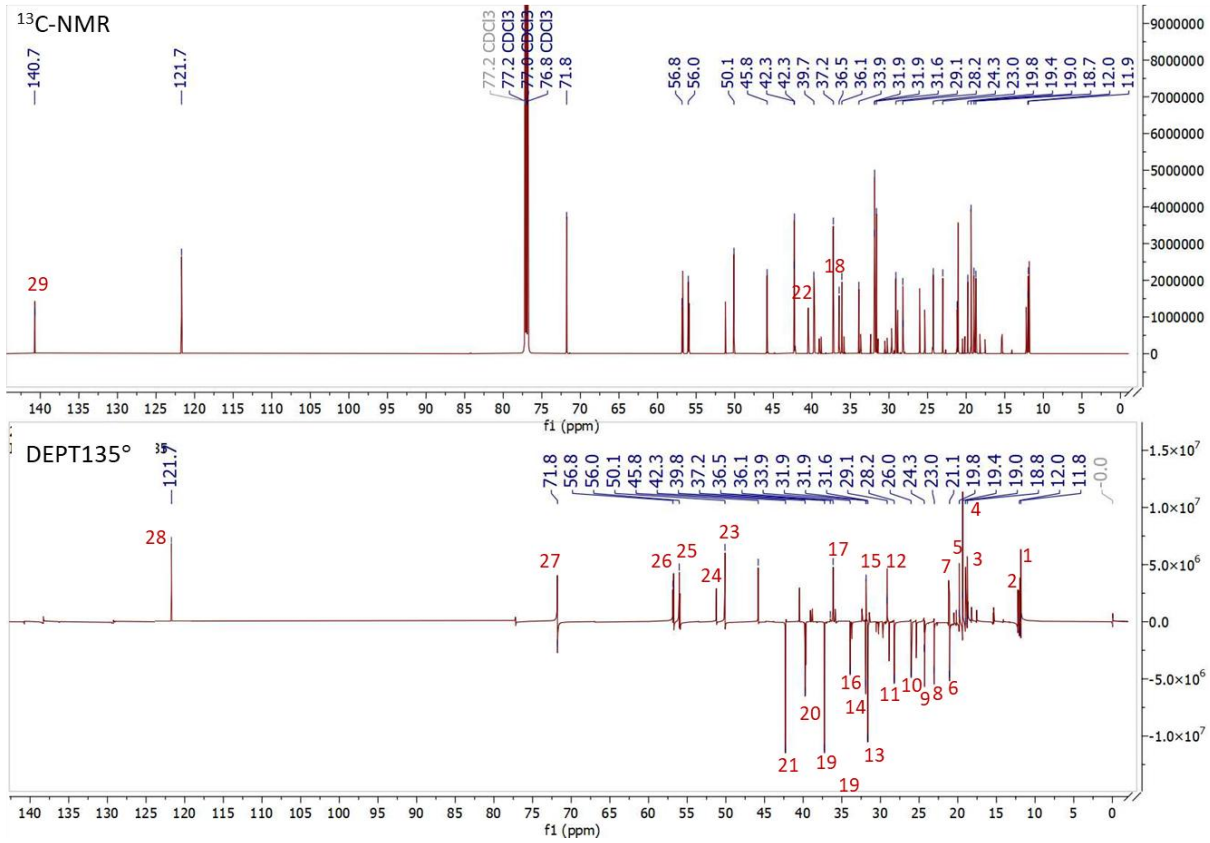

Figure S3 ^{13}C-NMR and DEPT spectrum from Compound **1**.

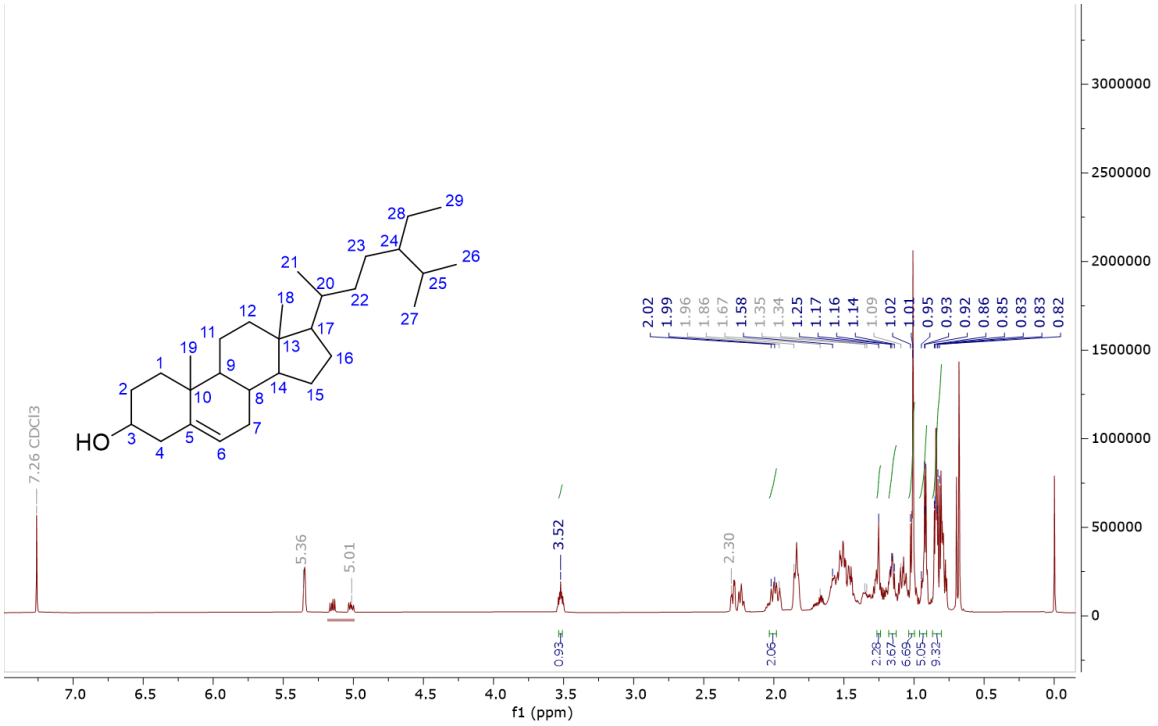

Figure S4 ^{1}H-NMR spectrum from Compound **1**.

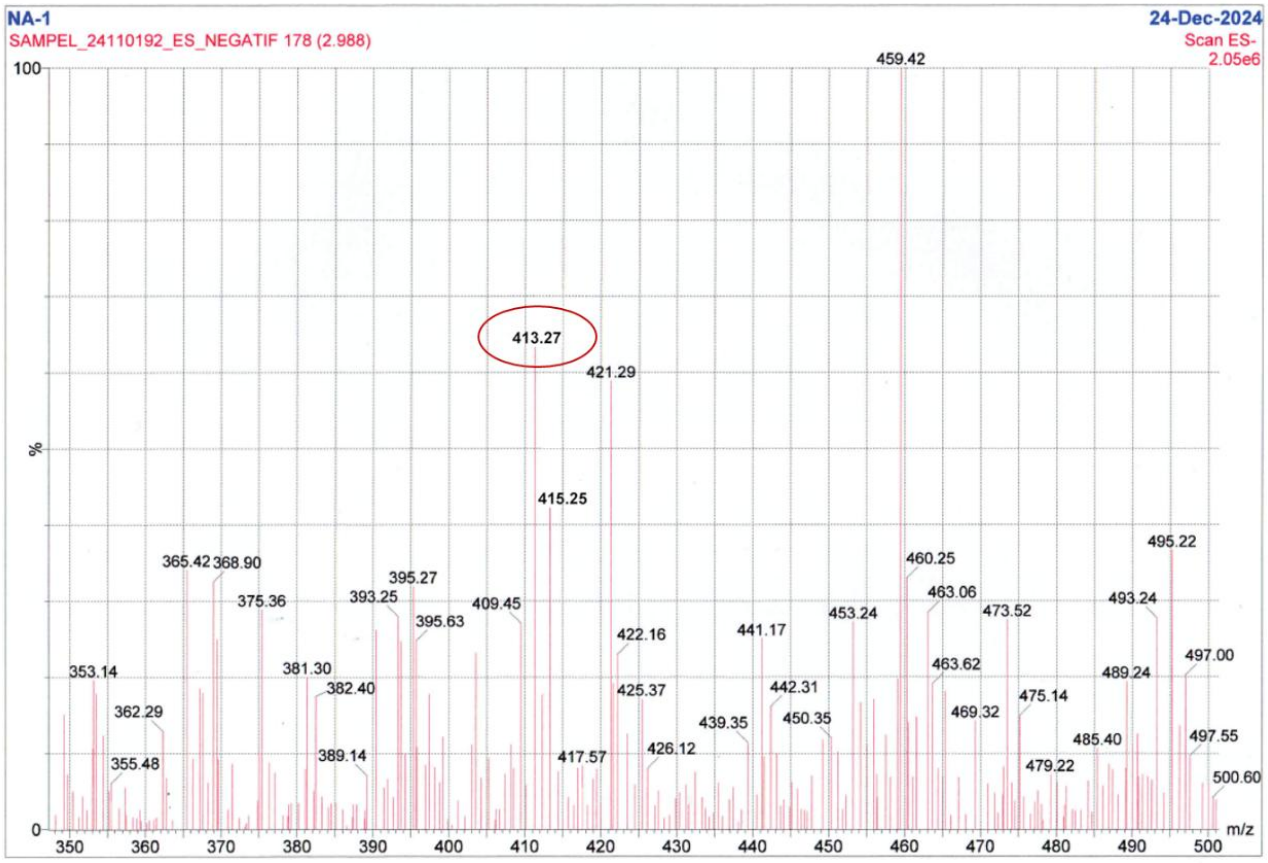

Figure S5 MS spectrum from Compound **1**.

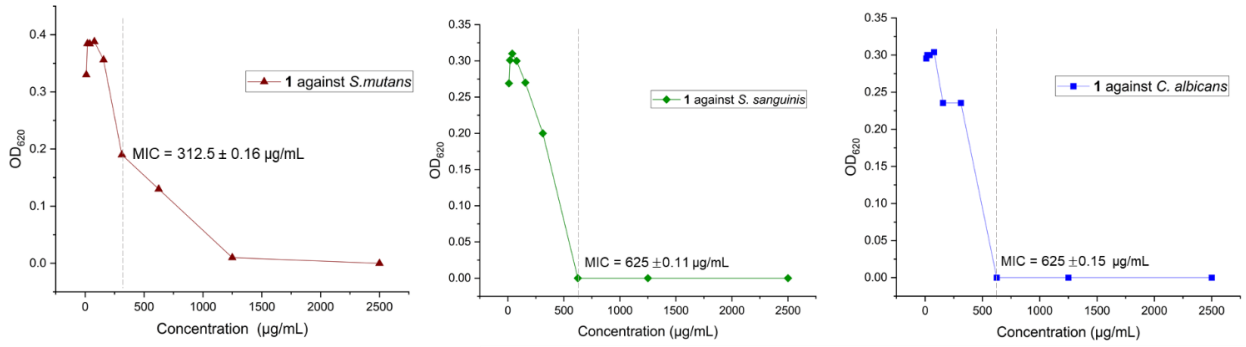

Figure S5 MIC curve of compound **1** against *S. mutans, S. sanguinis,* and *C. albicans*. The MIC is the lowest concentration that results in reduction of the viability of an inoculum of a microorganism.

Table S1 Inhibition zone of Fr.A-K against several microorganisms.

Fraction	Inhibition zone (mm) at 2% (v/v)		
	S. mutans	***S. sanguinis***	***C. albicans***
A	6,8	6.0	9
B	7.0	7.6	7.0
C	7.3	7.8	9.5
D	0	0	0
E	7.2	7.4	0
F	7.0	7.7	0
G	7.1	7.6	0
H	7,2	7.6	0
I	6,9	6,8	0
J	6,8	0	0
K	7,0	0	0
Positive control	14.5	14.0	15.0

Table S2 Comparison of ^{1}H-NMR and ^{13}C-NMR of compound **1** with β-sitosterol literature.

Carbon Position	Compound 1 ($CDCl_3$)			β-sitosterol Literature Data ($CDCl_3$) [1,2]		
	δ_C (ppm) (175 MHz)	**δ_H (ppm) (700 MHz)**	**DEPT**	**δ_C (ppm) (100 MHz)**	**δ_H (ppm) (400 MHz)**	**DEPT**
C-1	37.3	1.85 (m, 2H)	CH_2	37.4	1.85 (m, 2H)	CH_2
C-2	31.7	1.95 (m, 2H)	CH_2	31.8	1.95 (m, 2H)	CH_2
C-3	71.9	3.52 (m, 1H)	CH	72.0	3.55 (m, 1H)	CH
C-4	42.2	2.30 (m, 2H)	CH_2	42.4	2.38 (m, 2H)	CH_2
C-5	140.8	-	C	140.9	-	C
C-6	121.8	5.36 (m, 1H)	CH	121.9	5.37 (m, 1H)	CH
C-7	31.9	1.99 (m, 2H)	CH_2	32.1	1.99 (m, 2H)	CH_2
C-8	31.9	2.02 (m, 1H)	CH	31.9	2.00 (m, 1H)	CH
C-9	50.2	0.95 (m, 1H)	CH	50.3	0.94 (m, 1H)	CH
C-10	36.6	-	C	36.6		C
C-11	21.2	1.02 (m, 2H)	CH_2	21.2	1.02 (m, 2H)	CH_2
C-12	39.8	1.16 (m, 2H)	CH_2	39.9	1.16 (m. 2H)	CH_2
C-13	42.4	-	C	42.5		C
C-14	56	1.01 (m, 1H)	CH	56.9	1.00 (m. 1H)	CH
C-15	24.4	1.58 (m, 2H)	CH_2	28.4	1.58 (m, 2H)	CH_2
C-16	28.3	1.09 (m, 2H)	CH_2	28.4	1.09 (m, 2H)	CH_2
C-17	56.1	1.14 (m, 1H)	CH	56.2	1.12 (m, 1H)	CH
C-18	11.9	0.84 (s, 3H)	CH_3	12.1	0.85 (s. 3H)	CH_3
C-19	19.1	0.82 (s, 3H)	CH_3	19.4	0.82 (s. 3H)	CH_3
C-20	36.2	1.35 (m, 1H)	CH	36.3	1.35 (m, 1H)	CH

Carbon Position	Compound 1 ($CDCl_3$)			β-sitosterol Literature Data ($CDCl_3$) [1,2]		
	δ_C (ppm) (175 MHz)	**δ_H (ppm) (700 MHz)**	**DEPT**	**δ_C (ppm) (100 MHz)**	**δ_H (ppm) (400 MHz)**	**DEPT**
C-21	18.9	0.92 (d, *J*= 5,12 Hz, 3H)	CH_3	18.9	0.95 (d. 3H)	CH_3
C-22	33.9	1.34 (m, 2H)	CH_2	34.0	1.33 (m, 2H)	CH_2
C-23	26.1	1.16 (m, 2H)	CH_2	26.1	1.16 (m, 2H)	CH_2
C-24	45.9	0.94 (m, 1H)	CH	45.9	0.94 (m, 1H)	CH
C-25	29.2	1.67 (m, 1H)	CH	28.9	1.66 (m, 1H)	CH
C-26	21.3	0.83 (d, *J*= 11 Hz, 3H)	CH_3	21.4	0,83 (d, 3H)	CH_3
C-27	19.5	0.83 (d, 3H)	CH_3	19.2	0.84 (d, 3H)	CH_3
C-28	23.1	1.25 (m, 2H)	CH_2	23.2	1.25 (m, 2H)	CH_2
C-29	12.0	0.83 (m, 3H)	CH_3	12.1	0.85 (m, 3H)	CH_3

Table S3 RMSD data of compound **3**, fluconazole, and apo state of CYP51.

Variables	Mean	SD	Median	Median absolute deviation (MAD)
Compound **3**	1.637	0.202	1.646	0.219
Fluconazole	1.706	0.222	1.748	0.221
Apo	1.520	0.177	1.538	0.174